Title
INSTANTANEOUS GLOBAL OZONE BALANCE INCLUDING OBSERVED NITROGEN DIOXIDE

Author
Solomon, S.

Publication Date
1979-06-01

LBL-9607
Preprint

Lawrence Berkeley Laboratory
UNIVERSITY OF CALIFORNIA

Materials & Molecular Research Division

Submitted to Pure and Applied Geophysics

INSTANTANEOUS GLOBAL OZONE BALANCE INCLUDING OBSERVED NITROGEN DIOXIDE

Susan Solomon, Harold S. Johnston, Marta Kowalczyk, and Ivan Wilson

June 1979

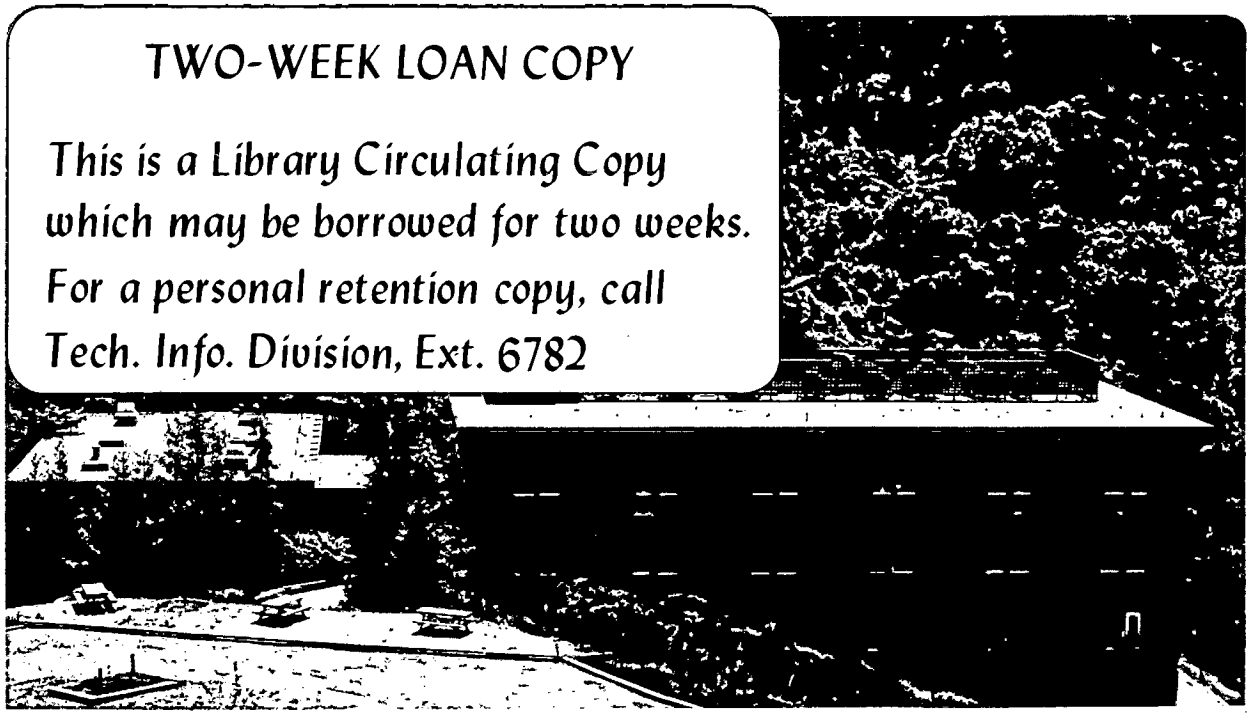

Prepared for the U. S. Department of Energy
under Contract W-7405-ENG-48

DISCLAIMER

LBL-9607

Instantaneous Global Ozone Balance Including Observed Nitrogen Dioxide

By

Susan Solomon, Harold S. Johnston, Marta Kowalczyk, and Ivan Wilson

Department of Chemistry, University of California, and Materials and Molecular Research Division, Lawrence Berkeley Laboratory, Berkeley, California 94720

Abstract

The catalytic destruction of stratospheric ozone by the oxides of nitrogen is believed to be an important part of the global ozone balance. The lack of sufficient measurements of NO_x concentrations has impeded efforts to quantify this process. Recent measurements of stratospheric nitrogen dioxide from ground-based stations as well as aircraft and balloons have provided a first approximation to a global distribution of NO_2 vertical columns at sunset. These observed vertical columns have been translated into time-dependent vertical NO_2 profiles by means of a one-dimensional atmospheric photochemical model. Using recent observations of air temperature and ozone along with this information, the independent instantaneous (one second) rates of ozone production from oxygen photolysis, $P(O_3)$, of ozone destruction from pure oxygen species (Chapman reactions) $L(O_x)$, and of ozone destruction by nitrogen oxides $L(NO_x)$ were estimated over the three dimensional atmosphere. These quantities are displayed as zonal average contour maps, summed over various latitude zones, summed over various altitude bands, and integrated globally between 15 and 45 km. Although the global summation between 15 and 45 km by no means tells the complete story, these numbers are of some interest, and the relative values are: $P(O_3)$, 100; $L(O_x)$, 15; $L(NO_x)$, 45 ± 15. It is to be emphasized that this relative NO_x contribution to the integrated ozone balance is not a measure of the sensitivity of ozone to possible perturbations of stratospheric NO_x; recent model results must be examined for current estimates of this sensitivity.

I. Introduction

The importance of the oxides of nitrogen in affecting the stratospheric ozone balance has been a subject of interest in atmospheric chemistry for several years (CRUTZEN, 1970). Recently, NOXON (1978, 1979) and NOXON et al. (1979) have presented measurements of the stratospheric column of nitrogen dioxide, NO_2, at numerous latitudes and seasons. There are now several NO_2 profiles up to the middle stratosphere observed from balloons (ACKERMAN et al., 1975; FONTANELLA et al., 1974; OGAWA, 1979; MURCRAY et al., 1974; HARRIES et al. 1976; EVANS et al., 1977; EVANS et al., 1978; GOLDMAN et al., 1978; DRUMMOND and JARNOT, 1978). DÜTSCH (1978) has reviewed all of the available data on the vertical ozone distribution measured with chemical sondes and one year of ozone data obtained by backscattered ultraviolet radiation from the Nimbus 4 satellite.

We have taken these recent measurements of temperature, ozone, and nitrogen dioxide; and using a photochemical model we have translated the observed NO_2 columns to time-dependent vertical profiles, which were then extended to global stratospheric distributions. We then examined the global distribution of the rate of NO_x catalyzed destruction of ozone by the method of instantaneous rates.

The method of instantaneous rates has been described previously (JOHNSTON and WHITTEN, 1973, 1975; JOHNSTON, 1975). Briefly the observed distribution of temperature, oxygen, ozone, and incoming solar radiation outside the atmosphere are used to calculate photolysis rates on a grid containing 1 km vertical intervals, 10° latitude intervals, and 15° longitude intervals. Rayleigh scattering and albedo effects are treated by the method of ISAKSEN et al. (1976). The concentration

of $O(^3P)$ is calculated at each grid point using the steady-state approximation. At each grid point three independent components of the global ozone balance were evaluated: (a) The rate of ozone production from the photolysis of oxygen, $P(O_3)$, which is 2 $j[O_2]$ as can be seen from the pair of reactions

$$\begin{array}{ll} O_2 + h\nu\ (\lambda < 242\ nm) \rightarrow O + O & \text{(slow)} \\ (O + O_2 + M \rightarrow O_3 + M) \times 2 & \text{(fast)} \\ \hline \text{net:}\quad 3\ O_2 + h\nu \rightarrow 2\ O_3 & \end{array} \qquad (1)$$

(b) The rate of ozone destruction by the pure oxygen family of reactions, $L(O_x)$, which is 2 $k[O][O_3]$ on the basis of

$$\begin{array}{ll} O_3 + h\nu\ (uv,\ vis) \rightarrow O_2 + O & \text{(fast)} \\ O + O_3 \rightarrow O_2 + O_2 & \text{(slow)} \\ \hline \text{net:}\quad 2\ O_3 + h\nu \rightarrow 3\ O_2 & \end{array} \qquad (2)$$

(c) The rate of ozone destruction by the oxides of nitrogen, $L(NO_x)$, which is 2 $k'[O][NO_2]$ as can be seen from

$$\begin{array}{ll} NO + O_3 \rightarrow NO_2 + O_2 & \text{(fast)} \\ O_3 + h\nu\ (uv,\ vis) \rightarrow O_2 + O & \text{(fast)} \\ NO_2 + O \rightarrow NO + O_2 & \\ \hline \text{net:}\quad 2\ O_3 + h\nu \rightarrow 3\ O_2 & \end{array} \qquad (3)$$

In each of the above cases the loss or production of ozone resulting from the catalytic cycle is given by the rate determining step in each cycle.

One might protest that the O_x, NO_x, HO_x, and ClX families of reactions are coupled, and as a consequence the ozone production and

losses cannot simply be identified as 2 $j[O_2]$, 2 $k[O][O_3]$, and 2 $k'[O][NO_2]$. It is true that the O_x, NO_x, HO_x, and ClX families are strongly coupled, but it is appropriate to review the nature of the coupling and to note what retains its identity during the interactions. Suppose the photochemistry of the stratosphere is represented by m chemical species, A_1, A_2 $\cdots$ A_m, and n photolytic and chemical reactions with rate constants, j_1, j_2, $\cdots$ k_n, at each grid point of the model. A change in the concentration of a chemical substance A_i may change the concentrations of many, perhaps all, other species. If changing A_i causes a change in local temperature, all temperature-dependent rate constants would be affected. If changing A_i causes a change in the ozone profile, the distribution of solar radiation in the atmosphere and the photolytic rate constants j would be altered. As an example, an increase in nitric oxide changes the concentrations of HO_x species through the reaction HOO + NO → HO + NO_2 and changes the concentrations of ClX species through the reaction ClO + NO → Cl + NO_2. Thus the concentrations of various species A_i are coupled to each other, and by feed-back mechanisms the values of temperature dependent rate constants may be affected. However, there are some things that are not changed when species concentrations are altered, in particular the identity of the n photochemical reactions in the model. The set of photochemical reactions can be expressed in terms of linear combinations of these reactions. With care, a set of linear combinations of reactions can be found such that the net effect of each is either (i) an increase in two molecules of ozone, (ii) a decrease in two molecules of ozone, or (iii) no change in ozone (JOHNSTON and PODOLSKE, 1978). Reactions (1), (2), and (3) represent such linear combinations of reactions.

The measured ozone and nitrogen dioxide concentrations are the observed results of all the various coupled chemical processes and of atmospheric transport. At each grid point of the sunlit atmosphere, three components of the ozone balance can be evaluated from $2\ j[O_2]_{obs}$, $2\ k[O]_{calc}[O_3]_{obs}$, and $2\ k'[O]_{calc}[NO_2]_{obs}$. These quantities have been zonally averaged, vertically summed, and expressed as total global rates and as global rates in 5 km altitude bands. In this work, then, we have examined the contributions made by NO_x and O_x processes to the natural global ozone balance.

II. Observational Data

DÜTSCH'S (1978) data were supplied as temperature and ozone partial pressures on a pressure grid from 0.5 to 250 mb, each 10 degrees of latitude from the south to the north pole, and for each month of the year. Data for three months were averaged to give seasonal averages, i.e., March, April, May; spring, etc. For each of the four seasons, the data were converted to ozone mixing ratios and ozone concentrations using the barometric equation to yield altitudes at 1 km intervals starting from the 250 mb level and interpolating between the given pressure levels. For altitudes below 250 mb, earlier distributions were used (DÜTSCH, 1969; JOHNSTON and WHITTEN, 1973). Examples of the global spring and winter temperature distributions are given in Figure 1. The corresponding ozone mixing ratios (ppbv) and concentrations in units of 10^9 molecules cm^{-3} are presented as Figures 2 and 3 respectively.

The concentration of atomic oxygen was calculated at each grid point of the atmosphere and for each of the four seasons. The orientation of the sun relative to the earth was that for spring and fall equinox and winter and summer solstice. A zonal average of the atomic oxygen concentration over daylight hours was obtained for each grid point of altitude and latitude, and representative results are given in Figure 4.

Observational data are now available that give a first approximation to the global distribution of stratospheric NO_2 (NOXON et al., 1979; NOXON, 1979). The measurements were made from the ground or from

aircraft during the twilight period using Rayleight-scattered sunlight from overhead. This gave changes in the NO_2, visible, absorption-spectrum through long optical paths in the stratosphere as the sun moved from 88° to 97° with respect to the vertical. The spectral changes during sunset (or sunrise) gave the value of the stratospheric NO_2 vertical column as primary information and gave an estimate of the altitude of maximum NO_2. In this article we interpret NOXON'S stratospheric NO_2 column as being that between 15 and 50 km.

At mid-latitudes, NOXON et al. (1979) reported AM and PM columns of nitrogen dioxide as well as the altitude of its maximum concentration. During the day the stratospheric NO_2 column increases by approximately a factor of two, presumably as the compounds N_2O_5, HNO_3, $ClONO_2$, and possibly $HOONO_2$ are photolyzed.

NOXON (1979) presented the global behavior of NO_2 in a series of figures. As a function of latitude, his Figure 1 gave representative measurements of the late afternoon vertical column of stratospheric NO_2. We read these points from the graph and listed them in Table 1. In NOXON'S Figure 2, the NO_2 columns at Cusco, Peru, 14°S, were given over a nine day period; the late afternoon columns read from the graph are in Table 1. At four stations (40°N, 49°N, 53°N, and 65°N) enough data were taken to provide 12 month variation of the NO_2 columns, and these data are given as NOXON'S Figure 3. For each of our four seasons (winter solstice, spring equinox, summer solstice and fall equinox), we read the value of the NO_2 column from NOXON'S smooth curve in his Figure 3, and these points are included in Table 1. Also the data points in NOXON'S Figure 6 are listed in Table 1. For the relatively

few NO_2 columns observed in the southern hemisphere, (SH), NOXON found a gross symmetry with respect to the corresponding season in the northern hemisphere, (NH). To extend the data base, we reflected all observed points in Table 1 to the other hemisphere with a six month phase shift. The points in Table 1 are plotted in Figure 5 to represent the observed NO_2 statospheric columns for spring (NH), fall (SH) and in Figure 6 to represent summer (SH), winter (NH).

The vertical distributions of stratospheric nitrogen dioxide as observed from balloons typically go from a lower altitude of 12 to 20 km to an upper altitude of 28 to 40 km. The profile measured by DRUMMOND and JARNOT (1978) extended from 20 to 50 km. Some of these measurements were made at sunset, some at sunrise, and some at noon. NOXON'S stratospheric NO_2 columns of Table 1 and Figures 5 and 6 refer to late afternoon conditions and essentially to the NO_2 between 15 and 50 km, and the column provided by the balloon profiles are not strictly comparable. We filled in the gaps in the lower stratosphere, or upper stratosphere, or both to give extended balloon profiles from 15 to 50 km by using estimates from the photochemical model. In the cases where the balloon profile did not correspond to late afternoon conditions, we ran the photochemical model from sunrise to sunset to obtain a model value for the PM/AM ratio for the NO_2 column. The values, typically about two, were used to scale the observed column to PM conditions. Table 2 contains the resulting columns from the observed NO_2 profiles and the value of the corresponding column scaled as described above. Each balloon study is labeled by a letter A through H in Table 2, and these letters appear as data points on Figures 5 and 6.

Entry A in Figure 5 is based on ACKERMAN et al. (1975) from 20 to 36 km, on FONTANELLA et al. (1974) from 15 to 20 km, and on a model-based extension from 36 to 50 km, and this balloon-based column agrees with or may be somewhat smaller than NOXON'S results. At the other extreme, HARRIES' column is far greater than NOXON'S column for the corresponding latitude and season, Figure 5 (JOHNSTON and PODOLSKE, 1978, pointed out that the NO_2 from HARRIES column destroyed ozone above 30 km much faster than it was produced by sunlight and was probably not representative of general conditions). The other observed PM nitrogen dioxide columns scaled to 15 to 50 km lie somewhat above NOXON'S NO_2 columns, although in general not more than the ± 20 percent error that NOXON estimated for his method.

Considering both NOXON'S results and the balloon results, we derived the lines in Figures 5 and 6 to use as the present estimate of the global and seasonal stratospheric NO_2 columns between 15 and 50 km. Certain sensitivity studies were carried out where the curves of Figures 5 and 6 were scaled by the factor 2/3 or by the factor 4/3.

III. Photochemical Model Calculations

Originally we intended to treat the NO_2 distribution 100 percent empirically, using (i) the vertical columns from Figures 5 and 6, (ii) two as a universal PM/AM ratio with linear change with time during the day at all altitudes, (iii) NOXON'S observed altitudes of maximum NO_2, and (iv) a Gaussian function (σ = 7 km) derived from balloon measurements to give the vertical NO_2 profile. This procedure was carried through for one calculation of global instantaneous rates. Its assumptions were tested against a time-dependent photochemical model, and the assumptions were not sustained. The rate of change of NO_2 between AM and PM was found not to be uniform with altitude. Model calculations do not yield an NO_2 profile which is Gaussian in shape. The rapid rise in the concentration of $O(^3P)$ with increasing altitude, as shown in Figure 4, causes the maximum rate of the $O + NO_2$ reaction to occur at a higher altitude than the maximum NO_2 concentration. In order to evaluate the global contribution of this process to the natural ozone balance, it is essential to know the nitrogen dioxide concentrations at high stratospheric altitudes, where there are few measurements. It was felt that model extrapolation of the NO_2 profile above the highest altitude of NO_2 measurement was more reliable than an empirical extrapolation from the limited set of observations. As a result of these considerations, we decided to take the observed PM vertical columns of NO_2 as primary data and to use a photochemical model to establish the PM/AM ratio, the change of NO_2 during the day, and the vertical distribution of the NO_2.

The model used includes one dimensional atmospheric motion and photochemistry; it was obtained from the Lawrence Livermore Laboratory as their 1974 model (CHANG, 1974; CHANG et al., 1974), and we modified it to include additional species and reactions. Twenty species are treated time-dependently (O_3, O, HO, HOO, H_2O, H_2O_2, N_2O, NO, NO_2, NO_3, N_2O_5, HNO_3, CH_4, CO, Cl, ClO, $ClONO_2$, HCl, CF_2Cl_2, $CFCl_3$) and three species are treated by steady-state approximations [$O(^1D)$, N, H]. A natural background of 2 ppbv of total chlorine is prescribed, including CF_2Cl_2 and $CFCl_3$ in lieu of natural CH_3Cl. The vertical eddy diffusion function of STEWART and HOFFERT (1975) is used. The differential equations for each atmospheric species are solved using the Gear method. The chemical reactions and rate constants are given in Table 3.

Model calculations were performed to obtain reference NO_2 profiles for three zones: polar, mid-latitude, and tropical regions. For the mid-latitude region, the model was run, using a constant sun at half intensity, for 30 years. DÜTSCH'S ozone was taken as the initial distribution, and runs were made with four different sets of boundary values for NO and NO_2. Each of these runs was followed by three days of diurnal calculations with a maximum time step of 200 sec and where the photolysis rates varied continually according to the computed solar angle and radiation flux. This produced four sets of stratospheric evening NO_2 profiles, for which the columns bracketed the range observed by NOXON. From these four profiles we derived linear interpolation factors that gave the NO_2 profile at any time of day starting from a given PM vertical column.

For tropical and polar regions, we could not expect a one-dimensional eddy-diffusion model to give reasonable results. Our goal is not to model ozone but only to find the shape of the stratospheric NO_2 profile. For this purpose it is worthwhile to re-examine the order of magnitude of the chemical relaxation time for various processes. At all altitudes NO and NO_2 attain a steady state, primarily but not exclusively by way of

$$NO_2 \underset{O_3}{\overset{h\nu\ (\lambda < 400\ nm)}{\rightleftharpoons}} NO$$

with a relaxation time of about 2 minutes. This rapidly exchanged pair ($NO_x = NO + NO_2$) interchanges with N_2O_5 and $ClONO_2$ with chemical relaxation times of the order of a day or a few days. NO_x interchanges with nitric acid

$$NO_2 \underset{h\nu,\ HO}{\overset{HO}{\rightleftharpoons}} HNO_3$$

with altitude-dependent characteristic chemical times of about one week to one month. The chemical and photochemical rate of destruction of N_2O in the stratosphere has a characteristic time of a few years, and the stratospheric residence time of NO_y ($NO + NO_2 + HNO_3 + ClONO_2 + 2\ N_2O_5$) is likewise a small number of years. From consideration of these relaxation times, we started model calculations in tropical and polar regions with observed profiles of slow species (O_3, H_2O, HNO_3), and for various assumed boundary values and initial profiles of NO_x we ran the model long enough to obtain a quasi-stationary state among the fast species (O, HO, HOO, H_2O_2, NO, NO_2, NO_3, N_2O_5, Cl, ClO, and $ClONO_2$).

This corresponded to seven days with constant sun at half intensity, followed by three days of 24 hours, time-dependent running of the model. A given NO_2 column would be interpolated between two of the late afternoon model columns, and the profiles during the previous day found by backing up in time and by interpolating between the two cases.

Two model NO_2 profiles at mid-latitude are compared with the observed profile between 20 and 50 km obtained by DRUMMOND and JARNOT (1978) in Figure 7. Curve A represents the observed NO_2 profile at 44°N, July, one hour after sunrise, and it corresponds to an integrated stratospheric column of 2.8×10^{15} molecules cm^{-2}. Curve B is a model profile corresponding to an integrated column of 2.4×10^{15} molecules cm^{-2}, and curve C represents an integrated column of 1.0×10^{15} molecules cm^{-2}. Moderately good agreement is obtained between the observed profile and the model calculations, especially in the important region between 30 and 45 km.

In order to further verify the high altitude behavior of the NO_2 chemistry which we have obtained from these model calculations, we have conducted a study of the solar proton event of 1972. This event has been previously discussed in detail (HEATH et al., 1977). It has been pointed out that the event introduced large quantities of NO in the polar stratosphere and therefore serves as a test for the theory that NO_x catalytically destroys ozone. Since the original study by HEATH et al. (1977) there have been major changes in several important rate constants. With 1978 rate constants (Table 3) we calculate ozone decreases in good agreement with the observed changes obtained by

satellite measurements above 35 km. As we show below, this is the region where the bulk of the NO_x catalyzed destruction of ozone occurs, and therefore the agreement obtained in this test case serves as some confirmation of the ability of the model to simulate this chemistry. A more detailed description of our study with particular emphasis on the differences in chemistry as compared to previous work (HEATH et al., 1977; FABIAN et al., 1979) will be presented elsewhere.

The model was checked against PM/AM ratios of the observed NO_2 concentration (EVANS et al., 1978). Between 20 and 30 km EVANS obtained a maximum PM/AM ratio of about 2, with lower values below, which varied on successive days. The model gives a PM/AM ratio of 1.8 in the 20 to 30 km region, with lower values below and above 30 km, which is similar to the observations.

This use of a model to translate a given NO_2 vertical column into a profile has some uncertainties due to atmospheric transport. If horizontal transport systematically has a different effect on NO_2 at different altitudes within a time span of a week or less, then the quasi-steady state obtained by the model among NO, NO_2, N_2O_5 and $ClONO_2$ will be systematically distorted.

Nitric acid is a major reservoir for the NO_x species, especially in the lower stratosphere. The photochemical relaxation time of HNO_3 is about a month in the lower stratosphere, it decreases with altitude, and it becomes short in the upper stratosphere. The 10 day integration time to set up quasi-steady state in tropical and polar regions would be adequate above about 25 km for HNO_3 but inadequate at substantially lower altitudes. We have examined the sensitivity of our calculation

to HNO_3 in the tropical region. Measurements of HNO_3 have been reported at various latitudes by LAZRUS and GANDRUD (1974), who used a filter collection technique, and by MURCRAY et al. (1975) who reported column measurements above 18 km based on infrared emission. Both authors observe a minimum in tropical regions. LAZRUS and GANDRUD reported tropical mixing ratios of HNO_3 that varied from 0.2 to 0.75 ppbm at 18 km, MURCRAY found a column of HNO_3 ranging from 1.0 to 5.4 x 10^{15} in the region 20°N to 20°S. Between the extremes of these observations, we have investigated the effect of two quite different tropical HNO_3 profiles produced by changing the initial distribution of HNO_3 and running the model for the usual seven plus three days. The results of this test are given below:

	Case 1	Case 2
Column of $HNO_3/10^{15}$ cm^{-2}	1.2	5.6
HNO_3 at 18 km/ppbm	0.36	2.2
Column rate of $O + NO_2$ reaction (5:30 pm)/10^{12} cm^{-2} sec^{-1}	3.8	4.0

From this study, it appears that the uncertainty in the shape of the NO_2 profile as a function of uncertainty in the HNO_3 profile is only a matter of about five percent on the inferred rate of the reaction ($O + NO_2 \rightarrow O_2 + NO$) in the tropical region.

IV. Results of Instantaneous Rate Calculations

Before presenting results of instantaneous rate calculations, a comparison and contrast will be given between these calculations and those of an atmospheric model. A model takes a set of chemical species, a list of chemical and photochemical reactions, a theory of atmospheric motions, and a mechanism for handling radiation. The model calculates atmospheric transport, photochemical reactions, and radiative balances. In a model calculation every result depends, with different sensitivity, on almost every parameter of the model. A proper model is a tool for predicting future events, including, for example, the effect of atmospheric perturbations.

The observed distributions of ozone, nitrogen dioxide, or other species is brought about by actual atmospheric processes, and the method of instantaneous rates starts with the measured consequences of real atmospheric motion, photochemistry, and radiation effects. To this extent, the method of instantaneous rates does not need to calculate atmospheric transport. As a consequence of its dependence on observed quantities, this method is concerned with <u>interpreting</u> the existing or past atmosphere and has no power of <u>predicting</u> the future atmosphere. Clearly the predictive role of the model is more valuable than the interpretative role of the method of instantaneous rates, although this method does have some unique and useful features.

Calculations are made of the distribution of solar radiation at every grid point, and the rates of some photochemical reactions are calculated at these grid points. The rates of ozone production from

O_2 photolysis, 2 $j[O_2]$, of ozone destruction from oxygen species, 2 $k[O][O_3]$, and of ozone destruction by nitrogen oxides, 2 $k'[O][NO_2]$, are calculated independently of each other and of other important processes that are occurring. Ozone losses to chlorine species (Cl, ClO) and to water species (H, HO, HOO) are obviously omitted. Also omitted is ozone production or loss to net transport in any given volume element. In an example discussed below, NO_x reactions destroy ozone in one region of the atmosphere at a rate five times the rate of photochemical production in that region. In this instance it is obvious that atmospheric transport has supplied ozone to a region that contains little or no solar radiation capable of producing ozone ($\lambda < 242$ nm) but that contains abundant visible radiation that dissociates ozone and drives the NO_x catalytic cycle. In other instances the relative role of atmospheric transport and photochemistry in affecting local ozone may not be apparent, and Figure 8 provides a reference map for this purpose. The "ozone replacement time" is the local ozone concentration divided by the local rate of oxygen photolysis (1)

$$\tau = [O_3]/2\ j[O_2] \qquad (4)$$

and this quantity is presented in Figure 8 where 2 $j[O_2]$ is the 24 hour average value. The ozone replacement times increase with decreasing altitude from about 10 hours in the upper stratosphere to several years in the lower stratosphere. Vertical transport times in the stratosphere over a 10 km altitude range are more or less a year; horizontal transport times over 10000 km range are also more or less a year. In these terms, ozone photochemistry is faster than ozone transport only above 25 to 35 km (latitude dependent).

About every two weeks solar radiation produces enough ozone, $2\ j[O_2]$, to equal that in the entire atmosphere. This large gross ozone formation is balanced by equally large ozone-destruction processes. The atmosphere as a whole is a closed system, and ozone transported from one region must eventually be destroyed somewhere. In this section global distributions of ozone formation and of ozone destruction by O_x and NO_x are given, but these distributions need to be examined in the light of Figure 8 and the time-scale of atmospheric motions to determine their magnitude relative to transport.

Contour lines for the daytime average nitrogen dioxide concentrations are presented as a function of altitude and latitude and for two seasons in Figure 9. The corresponding mixing ratios are shown in Figure 10. The two seasons are spring equinox (fall, SH; spring, NH) and winter solstice (summer, SH; winter, NH), and all remaining figures in this article are based on these two seasons. The NO_2 columns were assumed to be symmetrical between the two hemispheres for corresponding seasons. Temperature and ozone concentration are not symmetrical between the hemispheres. Instantaneous rate calculations were done for the other two seasons, summer solstice (winter, SH; summer, NH) and fall equinox (spring, SH; fall, NH), but these results are given here only in summary tabular form. Several features of NOXON'S measurements are evident in Figures 9 and 10: the low tropical NO_2 columns, the winter "cliff" above 50°N, and the "trough" in spring. The altitude of maximum concentration is typically close to 30 km, and the concentrations at the maximum are usually 1 to 3 x 10^9 molecules cm^{-3}. The altitude of maximum mixing ratio is about 35 km,

and the values at the maximum are about 6 to 12 ppbv. According to NOXON'S (1979) Figure 2, the altitude of maximum NO_2 concentration in the tropics varies between 20 and 28 km, whereas our model places the maximum at about 30 km. This difference in NO_2 heights in the tropics is the major disagreement between our model distribution of NO_2 and the indications of NOXON'S method.

The rate of ozone production, $P(O_3)$, from the photolysis of oxygen (1) is given by $2\ j_1[O_2]$. The distribution of radiation in the Schumann-Runge region was treated by the method of HUDSON and MAHLE (1972). The zonal average, or 24 hour average, rate of ozone production is given in Figure 11. The rate exhibits a broad maximum in the upper stratosphere, and an interesting feature is the large zonal-average value over the summer polar region. The rate of ozone destruction by pure oxygen species, $L(O_x)$, is given (2) by $2\ k[O][O_3]$, as an excellent approximation. The 24 hour average contours of this rate are shown in Figure 12.

The ratio of the two rates, $L(O_x)/P(O_3)$, is given by Figure 13. Above 42 km, the loss of ozone due to O_x reactions is about 25 percent of the rate of ozone production. This percentage rapidly decreases at lower altitude, reaching a region in the lower tropical stratosphere where ozone is produced 1000 times faster than it is destroyed by O_x reactions. The heavy lines in Figure 13 outline a region where O_x reactions destroy ozone at a rate comparable to ($L/P = 0.5$) to much faster than ($L/P = 5$) ozone is produced by solar radiation. At all four seasons this high fractional ozone destruction occurs in a region where the photochemical production of ozone is very slow. Ozone

production from O_2 occurs only from solar radiation at wavelengths less than 242 nm, which is strongly filtered by oxygen and ozone. Ozone destruction is brought about by oxygen atoms generated by ozone photolysis, which is driven by visible as well as ultraviolet radiation. Thus ozone, brought to a region by transport, undergoes slow photochemical destruction where the rate of ozone formation from O_2 photolysis is essentially zero.

The 24 hour average rate of ozone destruction by NO_x, $L(NO_x) = 2\ k[NO_2][O]$, is given by Figure 14. The maximum rate of ozone destruction by NO_x occurs at mid-latitudes between 30 and 40 km. Ozone is rapidly destroyed by this reaction at the rate of 10^6 molecules cm^{-3} s^{-1} in a band about 15 km wide stretching from pole-to-pole at the equinox. During the winter solstice, this band is 20 km wide over the summer pole and rapidly falls to zero as one approaches the winter pole.

The relative rate of ozone destruction by NO_x and ozone production from ozone photolysis is demonstrated by contour maps of the ratio $L(NO_x)/P(O_3)$, Figure 15. The heavy lines in this figure enclose the region of rapid rate of ozone destruction by NO_x; at one limit of this region NO_x destroys ozone half as fast as it is formed and the other extreme $L(NO_x)$ is five times as great as $P(O_3)$, which implies that NO_x is destroying ozone which was brought there by atmospheric transport from the "net ozone production region." In the summer-winter contour map, the zone of 50 percent or more ozone destruction lies in a band 10 km wide from the summer pole to 60°N. In the fall-spring case, the region of maximum destruction occurs in two large areas over mid-latitudes. Below the altitude of maximum ozone concentration in the

tropics (Figure 3), there is a region of some ozone formation where the rate is greater than 10^5 molecules cm^{-3} s^{-1} (Figure 11), but in this region there is almost no photochemical destruction of ozone by O_x (Figure 13) or by NO_x (Figure 15).

With a reduced number of contour lines, the map of the ratios $L(NO_x)/P(O_3)$ (Figure 14) are superimposed on the corresponding contour maps of ozone mixing ratios (Figure 2) to produce Figure 16. In region B, between the heavy lines, NO_x destroys ozone at least 50 percent as fast as it is formed. Points A represent mixing ratio maxima for ozone, and point C represents the maximum rate of O_2 photolysis. Region B lies across the region of maximum ozone mixing ratio for summer-winter, and it forms two large areas on each side of the ozone maximum mixing ratio for fall-spring conditions. If on the fall-spring map of Figure 16 one draws a line from point A to a point 18 km above the north pole, one finds an interesting picture for the possibilities of ozone transport from the photochemically active tropical middle stratosphere to the photochemically inert lower polar stratosphere. From the equator to about 40°N along this line, the rate of ozone production from O_2 photolysis is much faster than NO_x (or O_x) ozone destruction. Where this line crosses into region B, that of large fractional ozone destruction by NO_x, the absolute rate of ozone formation and destruction is low.

The part of region B in Figure 16 that extends as a narrow band below 20 km and through the troposphere is of no importance. This region involves very slow rates of oxygen photolysis and ozone production (Figures 8, 11), and the ozone distribution is dominated by atmospheric transport and by methane-NO_x smog reactions. Above 40 km

the ozone mixing ratios decrease with increasing altitude, the direction of ozone flux is presumably upwards, and the ozone destruction rate by NO_x also decreases with altitude. In this region ozone destruction by HO_x and ClX reactions become rapid.

The relative role of the pure oxygen species and the oxides of nitrogen in the global ozone balance is examined in Tables 4 and 5. The 24 hour average column rates between 15 and 45 km for ozone photochemical production $P(O_3)$, for ozone destruction by O_x reactions $L(O_x)$, and for ozone destruction by NO_x reactions $L(NO_x)$ are listed for each latitude between 80°S and 80°N in Table 4. For fall-spring conditions, the rate of ozone production at 80°N or 80°S is very slow (about 10 percent of that at the equator), and the destruction rates, $L(O_x) + L(NO_x)$, are about twice as fast as the photochemical production. At mid-latitudes (30° - 60°) the 15 to 45 km column rate of ozone destruction by O_x is about 14 percent and that by NO_x reactions is about 55 percent of the rate of ozone production. In tropical regions the percentages are 14 for $L(O_x)$ and 35 for $L(NO_x)$.

The global sums of $P(O_3)$, $L(O_x)$, and $L(NO_x)$ over various altitude bands of 5 km width are given in Table 5. Between 45 and 50 km the role of NO_x is quite small, $L(NO_x)$ being only seven percent of $P(O_3)$; over this range $L(O_x)$ is 23 percent of $P(O_3)$. Between 40 and 45 km, the O_x and NO_x reactions are about equally important in balancing ozone, and each destroys ozone about 25 percent as fast as it is produced. Between 30 and 40 km, the O_x reactions destroy ozone about 10 percent as fast as it is produced, and NO_x destroys about 57 percent. Between 25 and 30 km, $L(O_x)$ is six percent of $P(O_3)$, and $L(NO_x)$ is 35 percent.

Below 25 km both the rate of photochemical production of ozone and its destruction by O_x and NO_x become slow. Over the range 15 to 45 km on the global scale (compare JOHNSTON, 1975) the O_x reactions destroy 15 percent of the photochemically produced ozone and NO_x reactions destroy 43 percent for the fall-spring season. This total percentage of 58 leaves ample room for major effects by HO_x and Cl_x reactions.

The global role of NO_x in destroying ozone between 15 and 45 km is explored as a function of season in Table 6. Ozone destruction by NO_x is 43 percent of $P(O_3)$ in spring, 50 percent in summer, 39 percent in fall, and 43 percent in winter of the northern hemisphere. The average of these four seasons is 44 percent. The inventory of NO_2 in the sunlit half of the globe is about 1.3×10^{34} molecules, with some apparent seasonal changes.

A sensitivity study was carried out in which the PM nitrogen dioxide columns of Figures 5 and 6 were scaled by the factor 2/3 and by the factor 4/3. Some of the results are given in Table 7. NOXON estimated his NO_2 columns to be accurate to ± 20 percent. We have taken ± 33 percent in order to embrace most of the balloon soundings and to be somewhat conservative. For 2/3 the standard NO_2 columns, NO_x destroyed 29 percent of the global ozone produced from 15 to 45 km; for 4/3, NO_x destroyed 63 percent of the global ozone produced over this altitude interval. On the basis of the observed NO_2 columns, we estimate that the global rate of ozone destruction by NO_x is 45 ± 15 percent of the rate of ozone formation from oxygen photolysis between 15 and 45 km. However, one should take the rate of ozone destruction by NO_x from Figures 14-16 and Tables 4-6, rather than from the single number 45 ± 15 percent, which is averaged over many different regions.

This single number for the effect of nitrogen oxides on stratospheric ozone should be used with great caution. Emphatically, it is not an index for the sensitivity of stratospheric ozone to a perturbation by added NO_x. At present model calculations predict that an increase of stratospheric NO_x would decrease ozone in the upper stratosphere, would increase ozone in the lower stratosphere, and would have only a small effect of uncertain sign on the total ozone column (RUNDEL et al., 1978).

NOXON'S measurements and these calculations show that the mid-latitude region is not representative of the global average so far as NO_2 column and the NO_x rate of ozone destruction is concerned. The concentrations of NO_2 and the ozone destruction rates $L(NO_x)$ are higher in mid-latitude than in the tropics on one side or in the polar region on the other side. This observation is relevant to the degree that one-dimensional photochemical models can be verified by comparison with observations made at mid-latitudes.

This study of instantaneous rates omitted several minor sources of ozone formation, ozone destruction by O_x, and ozone destruction by NO_x (JOHNSTON and PODOLSKE, 1978). The most important source of ozone formation that is omitted is that from the methane-NO_x smog reaction. This smog reaction is an important local source of ozone below but not above 20 km. The present study is primarily concerned with the fast photochemical formation and destruction of ozone above 25 km, and the smog reactions are slow in this context. Ozone is also destroyed by the reaction of singlet atomic oxygen with ozone, but this small effect was omitted. Ozone is destroyed by another NO_x catalytic cycle starting

with the reaction $NO_2 + O_3 \rightarrow NO_3 + O_2$ and rate limited by the photolysis of the nitrate free radical to give nitric oxide, $NO_3 + h\nu \rightarrow NO + O_2$. Using GRAHAM and JOHNSTON'S (1978) quantum yields for this reaction, we have found that this cycle destroys 0.03 percent of the ozone produced globally from oxygen photolysis. However from one to 10 km, the globally integrated daytime rate is about 1×10^{28} molecules s^{-1}, which is large enough to be of importance in the troposphere where photochemistry is slow (compare CHAMEIDES and WALKER, 1976). The reaction $HOO + NO \rightarrow HO + NO_2$ is an important mechanism whereby an increase in the concentration of NO_x species affects the concentrations of HO_x species with consequent changes in a number of reaction rates. This strong coupling between the concentrations of various species does not constitute direct ozone formation or destruction, and this reaction is appropriately not included in the calculations of instantaneous rates where the concentration of NO_2 is observed.

In this calculation of instantaneous rates, the three quantities $P(O_3)$, $L(O_x)$, and $L(NO_x)$ are independent and are derived from different sets of atmospheric measurements. There was no need to include the several catalytic cycles whereby HO_x and ClX destroy ozone, although if we had enough atmospheric measurements of HOO and of ClO these calculations could be made. The global balance of ozone production against all modes of ozone destruction based on observed key species is a necessary condition for verifying the completeness of mechanisms of

stratospheric photochemistry. We look forward to the time when there are sufficient measurements of ClO and HOO in the stratosphere for calculations such as these to be made on the effects of ClX and HO_x on the global ozone balance.

Acknowledgment

This work was supported by the Division of Chemical Sciences, Office of Basic Energy Sciences, U.S. Department of Energy under contract No. W-7405-Eng-48. We especially thank the Lawrence Livermore Laboratory Atmospheric Kinetics Group for generously giving us a complete copy of their 1974 atmospheric model, which we have expanded and up-dated for use here. We are grateful to Professor H. U. DÜTSCH for supplying us with tables of atmospheric temperature and ozone data. We are grateful to Dr. J. B. KERR for sending us tables of data that had appeared only as figures [EVANS et al., 1978].

References

ACKERMAN, M., FONTANELLA, J. C., FRIMOUT, D., GIRARD, A., LOUISNARD, N., and MULLER, C. (1975), Simultaneous Measurements of NO and NO_2 in the Stratosphere, Planet. Space Sci. 23, 651-660.

CHAMEIDES, W. C., and WALKER, J. G. (1976), A Time Dependent Photochemical Model for Ozone Near the Ground, J. Geophys. Res. 81, 413-420.

CHAN, W. H., USELMAN, W. M., CALVERT, J. G., and SHAW, J. A. (1977), The Pressure Dependence of the Rate Constant for the Reaction HO + CO → H + CO_2, Chem. Phys. Lett. 45, 240-243.

CHANG, J. S. (1974), Simulations, Perturbation and Interpretations, Proceedings of the Third Conference on CIAP, U. S. Department of Transportation, DOT-TSC-OST-74-15, 330-341.

CHANG, J. S., HINDMARSCH, A. C., and MADSEN, N. K., Simulations of Chemical Kinetics and Transport in the Stratosphere, in Stiff Differential Systems, (R. A. Willoughky, Ed., Plenum, New York, 1974), pp. 51-65.

CONNELL, P. and JOHNSTON, H. S. (1979), The Thermal Dissociation of N_2O_5 in N_2, submitted to Geophys. Res. Lett.

COX, R. A. (1978), Kinetics of HO_2 Radical Reactions of Atmospheric Interest, Symposium on the Geophysical Aspects and Consequences of Changes in the Composition of the Stratosphere, Toronto, World Meteorological Organization, Publication No. 511.

CRUTZEN, P. J. (1970), The Influence of Nitrogen Oxides on the Atmospheric Ozone Content, Quart. J. Roy. Meteorol. Soc. 96, 320-325.

DRUMMOND, J. R., and JARNOT, R. F. (1978), Infra-red Measurements of Stratospheric Composition. II. Simultaneous NO and NO_2 Measurements, Proc. R. Soc. Lond. A 364, 237-254.

DÜTSCH, H. U., Atmospheric Ozone and Ultraviolet Radiation, World Survey of Climatology, (Vol. 4, D. F. Rex, Ed., Elsevier Publishing Company, Amsterdam, London, New York, 1969), pp. 383-432.

DÜTSCH, H. U. (1978), Vertical Ozone Distribution on a Gobal Scale, Pure Appl. Geophys. 116, 511-529.

EVANS, W. F. J., KERR, J. B., McELROY, C. T., O'BRIEN, R. S., RIDLEY, B. A., and WARDLE, D. I. (1977), The Odd Nitrogen Mixing Ratio in the Stratosphere, Geophys. Res. Lett. 4, 235-238.

EVANS, W. F. J., FAST, H., KERR, J. B., McELROY, C. T., O'BRIEN, R. S., and WARDLE, D. I. (1978), Stratospheric Constituent Measurements from Project Stratoprobe, Symposium on the Geophysical Aspects and Consequences of Changes in the Composition of the Stratosphere, Toronto, World Meteorological Organization, Publication No. 511.

FABIAN, P., PYLE, J. A., and WELLS, R. J. (1979), The August 1972 Solar Proton Event and the Atmospheric Ozone Layer, Nature 277, 458-460.

FONTANELLA, J. C., GRAMONT, L., and LOUISNARD, N. (1974), Vertical Distribution of NO, NO_2 and HNO_3 as Derived from Stratospheric Absorption Spectra, Proceedings of the Third Conference on CIAP, U. S. Department of Transportation, DOT-TSC-OST-74-15, 454-457, and Appl. Opt. 14, 825-828,

GOLDMAN, A., FERNWALD, F. G., WILLIAMS, W. S., and MURCRAY, D. G. (1978), Vertical Distribution of NO_2 in the Stratosphere as Determined from Balloon Measurements of Solar Spectra in the 4500 Å Region, Geophys. Res. Lett. 5, 320-325.

GRAHAM, R. A., and JOHNSTON, H. S. (1978), The Photochemistry of NO_3 and the Kinetics of the N_2O_5-O_3 System, J. Phys. Chem. 82, 254-268.

HAMPSON, R. F., and GARVIN, D. (1977), Reaction Rate and Photochemical Data for Atmospheric Chemistry, NBS Special Publication 513.

HARRIES, J. E., MOSS, D. G., SWANN, N. R. W., NEILL, G. F., and GILDWANG, P. (1976), Simultaneous Measurements of H_2O, NO_2 and HNO_3 in the Daytime Stratosphere from 15 to 35 km, Nature 259, 300-302.

HEATH, D. F., KRUEGER, A. J., and CRUTZEN, P. J. (1977), Solar Proton Event: Influence on Stratospheric Ozone, Science 197, 886-889.

HOWARD, C. J. (1978), Recent Developments in Atmospheric HO_2 Chemistry, Symposium on the Geophysical Aspects and Consequences of Changes in the Composition of the Stratosphere, Toronto, World Meteorological Organization, Publication No. 511.

HUDSON, R. D., and MAHLE, S. H. (1972), Photodissociation Rates of Molecular Oxygen in the Mesosphere and Lower Thermosphere, J. Geophys. Res. 77, 2902-2914.

ISAKSEN, I. S. A., MIDTBÖ, K., DUNDE, J., and CRUTZEN, P. J. (1976), A Simplified Method to Include Molecular Scattering and Reflection in Calculations of Photon Fluxes and Photodissociation Rates, Institute for Geophysics, University of Oslo, Oslo, Norway, Report 20, pp. 1-21.

JOHNSTON, H. S., and WHITTEN, G. (1973), Instantaneous Photochemical Rates in The Global Stratosphere, Pure Appl. Geophys. 106-108, 1468-1489.

JOHNSTON, H. S., and WHITTEN, G. (1975), Chemical Reactions in the Atmosphere as Studied by the Method of Instantaneous Rates, Int. J. Chem. Kinet., Symposium No. 1, 1-26.

JOHNSTON, H. S. (1975), Global Ozone Balance in the Natural Stratosphere, Rev. Geophys. Space Phys. 13, 637-649.

JOHNSTON, H. S., and PODOLSKE, J. (1978), Interpretations of Stratospheric Photochemistry, Rev. Geophys. Space Phys. 16, 491-519.

LAZRUS, A. L., and GANDRUD, B. W. (1974), Distribution of Stratospheric Nitric Acid Vapor, J. Atmos. Sci. 31, 1102-1108.

MURCRAY, D. G., GOLDMAN, A., WILLIAMS, W. J., MURCRAY, F. H., BROOKS, J. N., VAN ALLEN, J., STOCKEN, R. N., KOSTERS, J. J., BARKER, D. B., and SNIDER, D. E. (1974), Recent Results of Stratospheric Trace-Gas Measurements from Balloon-Borne Spectrometers, Proceedings of the Third Conference on CIAP, U. S. Department of Transportation, DOT-TSC-OST-74-15, pp. 184-192.

MURCRAY, D. G., BARKER, D. B., BROOKS, J. N., GOLDMAN, A., and WILLIAMS, W. J. (1975), Seasonal and Latitudinal Variation of the Stratospheric Concentration of HNO_3, Geophys. Res. Lett. 2, 223-225.

NOXON, J. F. (1978), Stratospheric NO_2 in the Antarctic Winter, Geophys. Res. Lett. 5, 1021-1022.

NOXON, J. F., WHIPPLE, E. C. JR., and HYDE, R. S. (1979), Stratospheric NO_2. I. Observational Method and Behavior at Mid-Latitude, J. Geophys. Res., in press.

NOXON, J. F. (1979), Stratospheric NO_2. II. Global Behavior, J. Geophys. Res., in press.

OGAWA, T. (1979), Private Communication.

RUNDEL, R. D., BUTLER, D. M., and STOLARSKI, R. S. (1978), Uncertainty Propagation in a Stratospheric Model. 1. Development of a Concise Stratospheric Model, J. Geophys. Res. 83, 3063-3073.

STEWART, R. W., and HOFFERT, M. I. (1975), A Chemical Model of the Troposphere and Stratosphere, J. Atmos. Sci. 32, 195-210.

Table 1. Vertical column of stratospheric nitrogen dioxide in units of 10^{15} molecules cm^{-2} as read from Figures 1, 2, 3, and 6 of NOXON (1979).

Season	NOXON Fig.	Date	Lat.	$\frac{NO_2}{10^{15}}$	Season	NOXON Fig.	Date	Lat.	$\frac{NO_2}{10^{15}}$
SP	1	4/75	77 N	4.9	SU	1	7/75	82 N	6.9
			63 N	2.8				76 N	6.1
			48 N	2.8				69 N	5.3
			43 N	4.6				59 N	5.4
		3/77	41 N	3.9				53 N	5.2
			37 N	3.7				40 N	5.7
			27 N	3.1		3		65 N	5.1
			17 N	2.3				53 N	4.4
		10/76	12 S	2.2				49 N	4.6
			31 S	4.4				40 N	4.9
			35 S	5.5	W	1	2/77	57 N	1.3
	3		65 N	1.9				56 N	1.2
			53 N	1.9				55 N	1.4
			49 N	2.3				52 N	1.4
			40 N	3.9				51 N	1.1
F	2	3/77	14 S	2.6				48 N	1.1
				2.5				47 N	2.3
				2.6				46 N	1.9
				2.5				45 N	3.2
				2.2				44 N	3.5
				2.1				43 N	3.8
				2.9		3		65 N	1.3
	1	10/76	44 N	3.6				53 N	1.4
			42 N	4.2				49 N	2.7
			40 N	3.5				40 N	2.3
			20 N	3.2		6	2/77	56 N	1.4
	3		65 N	4.0				49 N	1.1
			53 N	4.0				44 N	3.0
			49 N	5.0				40 N	3.7
			40 N	4.5				30 N	3.8

Table 2. Observations of stratospheric nitrogen dioxide vertical columns from balloons. C_{NO_2} in units of 10^{15} molecules cm^{-2}.

Item in Figs. 5, 6	Lat. °N	Mo/Yr	Range of OBS km	Time	C_{NO_2} OBS	C_{NO_2}, PM 15-50 km	Reference
A	44	5/74	20-36	PM	2.0 to 3.2		ACKERMAN et al. (1975)
			15-20	PM	0.4 to 0.8	2.4 to 4.1	FONTENELLA et al. (1974)
B	40	5/78	20-35	PM	4.8	5.9	OGAWA (1979)
C	32	9/73	18-28	PM	2.3	4.4	MURCRAY et al. (1975)
D	44	9/74	24-35	NOON	4.7	8.4	HARRIES et al. (1976)
E	59	7/74	15-35	NOON	5.4	7	EVANS et al. (1977)
F	52	8/76	15-35	PM	6.3	6.6	EVANS et al. (1978)
		8/76	15-35	PM	5.6	5.9	
		8/76	15-31	PM	5.0	6.1	
G	32	2/77	20-42	PM	4.6	4.9	GOLDMAN et al. (1978)
H	44	6/75	20-50	AM	2.8	6.0	DRUMMOND and JARNOT (1979)

Table 3. List of reactions.

Reaction Rates [rate constants taken from HAMPSON and GARVIN (1977) except as noted].

$O + O_2 + M \rightarrow O_3 + M$	$1.07 \cdot 10^{-34}\ e^{(510/T)}$	
$O_3 + O \rightarrow 2\ O_2$	$1.9 \cdot 10^{-11}\ e^{(-2300/T)}$	
$O_3 + NO \rightarrow NO_2 + O_2$	$2.1 \cdot 10^{-12}\ e^{(-1450/T)}$	
$N_2O + O(^1D) \rightarrow N_2 + O_2$	$5.5 \cdot 10^{-11}$	
$N_2O + O(^1D) \rightarrow 2\ NO$	$5.5 \cdot 10^{-11}$	
$N + O_2 \rightarrow NO + O$	$5.5 \cdot 10^{-12}\ e^{(-3220/T)}$	
$N + NO \rightarrow N_2 + O$	$8.2 \cdot 10^{-11}\ e^{(-410/T)}$	
$N + NO_2 \rightarrow 2\ NO$	$6.0 \cdot 10^{-12}$	
$H_2O + O(^1D) \rightarrow 2\ OH$	$2.3 \cdot 10^{-10}$	
$CH_4 + O(^1D) \rightarrow OH + 2\ HO_2 + CO$	$1.3 \cdot 10^{-10}$	
$OH + O_3 \rightarrow O_2 + HO_2$	$1.5 \cdot 10^{-12}\ e^{(-1000/T)}$	
$O(^3P) + OH \rightarrow H + O_2$	$1.0 \cdot 10^{-10}\ e^{(-250/T)}$	
$HO_2 + O_3 \rightarrow OH + 2\ O_2$	$1.4 \cdot 10^{-14}\ e^{(-590/T)}$	HOWARD (1978)
$O(^3P) + HO_2 \rightarrow OH + O_2$	$1.0 \cdot 10^{-10}\ e^{(-250/T)}$	
$H + O_2 + M \rightarrow HO_2 + M$	$2.08 \cdot 10^{-32}\ e^{(290/T)}$	
$H + O_3 \rightarrow OH + O_2$	$1.42 \cdot 10^{-10}\ e^{(-478/T)}$	
$HO_2 + HO_2 \rightarrow H_2O_2 + O_2$	$3.9 \cdot 10^{-14}\ e^{(1245/T)}$	COX (1978)
$OH + HO_2 \rightarrow H_2O + O_2$	$5.0 \cdot 10^{-11}$	
$OH + NO_2 + M \rightarrow HNO_3 + M$	$4 \cdot 10^{-12} \cdot M/(1.12 \cdot 10^{18} + M)$	
$OH + HNO_3 \rightarrow H_2O + NO_3$	$8.0 \cdot 10^{-14}$	
$OH + H_2O_2 \rightarrow HO_2 + H_2O$	$1.0 \cdot 10^{-11}\ e^{(-750/T)}$	
$N_2 + O(^1D) + M \rightarrow N_2O + M$	$3.5 \cdot 10^{-37}$	
$N + NO_2 \rightarrow N_2O + O(^3P)$	$2.0 \cdot 10^{-11}\ e^{(-800/T)}$	
$NO + O(^3P) + M \rightarrow NO_2 + M$	$1.55 \cdot 10^{-32}\ e^{(584/T)}$	
$NO + HO_2 \rightarrow NO_2 + OH$	$3.3 \cdot 10^{-12}\ e^{(254/T)}$	HOWARD (1978)
$H_2 + O(^1D) \rightarrow OH + H$	$2.7 \cdot 10^{-10}$	

Table 3 (continued)

Reaction Rates

$OH + OH \rightarrow H_2O + O(^3P)$	$1.0 \cdot 10^{-11}\ e^{(-550/T)}$	
$N + O_3 \rightarrow NO + O_2$	$5.0 \cdot 10^{-12}\ e^{(-650/T)}$	
$NO_2 + O_3 \rightarrow NO_3 + O_2$	$1.23 \cdot 10^{-13}\ e^{(-2470/T)}$	
$OH + CH_4 \rightarrow H_2O + CO + 2\ HO_2$	$2.36 \cdot 10^{-12}\ e^{(-1710/T)}$	
$OH + OH + M \rightarrow H_2O_2 + M$	$1.25 \cdot 10^{-32}\ e^{(900/T)}$	
$O(^3P) + H_2O_2 \rightarrow OH + HO_2$	$2.75 \cdot 10^{-12}\ e^{(-2125/T)}$	
$Cl + O_3 \rightarrow ClO + O_2$	$2.7 \cdot 10^{-11}\ e^{(-257/T)}$	
$ClO + O(^3P) \rightarrow Cl + O_2$	$7.7 \cdot 10^{-11}\ e^{(-130/T)}$	
$ClO + NO \rightarrow Cl + NO_2$	$2.2 \cdot 10^{-11}$	
$Cl + CH_4 \rightarrow HCl + CO + 2\ HO_2$	$7.3 \cdot 10^{-12}\ e^{(-1260/T)}$	
$Cl + H_2 \rightarrow HCl + H$	$4.9 \cdot 10^{-11}\ e^{(-2340/T)}$	
$Cl + HO_2 \rightarrow HCl + O_2$	$3.0 \cdot 10^{-11}$	
$HCl + OH \rightarrow Cl + H_2O$	$3.0 \cdot 10^{-12}\ e^{(-425/T)}$	
$HCl + O \rightarrow Cl + OH$	$1.14 \cdot 10^{-11}\ e^{(-3370/T)}$	
$ClO + NO_2 + M \rightarrow ClONO_2 + M$	$3.3 \cdot 10^{-23} \cdot T^{-3.34} / (1 + 8.7 \cdot 10^{-9} \cdot T^{-.6} \cdot M^{.5})$	
$ClONO_2 + O \rightarrow ClO + NO_3$	$4.5 \cdot 10^{-12}\ e^{(-840/T)}$	
$CF_2Cl_2 + O(^1D) \rightarrow Cl + ClO$	$2.0 \cdot 10^{-10}$	
$CFCl_3 + O(^1D) \rightarrow 2\ Cl + ClO$	$2.0 \cdot 10^{-10}$	
$NO_2 + NO_3 + M \rightarrow N_2O_5 + M$		CONNELL and JOHNSTON (1979)
$N_2O_5 \rightarrow NO_2 + NO_3$		
$NO + NO_3 \rightarrow 2\ NO_2$	$1.87 \cdot 10^{-11}$	
$NO_2 + NO_3 \rightarrow NO + O_2 + NO_2$	$2.5 \cdot 10^{-14}\ e^{(-1127/T)}$	
$NO_3 + O \rightarrow NO_2 + O_2$	$1.0 \cdot 10^{-11}$	
$NO_3 + NO_3 \rightarrow 2\ NO_2 + O_2$	$8.5 \cdot 10^{-13}\ e^{(-2450/T)}$	
$CO + OH \rightarrow CO_2 + H$	$1.4 \cdot 10^{-13} + 7.33 \cdot 10^{-33} \cdot M$	CHAN et al. (1977)
$Cl + HNO_3 \rightarrow HCl + NO_3$	$1.0 \cdot 10^{-11}\ e^{(-2170/T)}$	

Table 3 (continued)

Photolysis Reactions

$O_2 + h\nu \rightarrow 2\ O(^3P)$	HUDSON and MAHLE (1972)
$O_3 + h\nu \rightarrow O + O_2$	
$O_3 + h\nu \rightarrow O(^1D) + O_2$	
$NO_2 + h\nu \rightarrow NO + O$	
$N_2O + h\nu \rightarrow N_2 + O$	
$NO + h\nu \rightarrow N + O$	
$HNO_3 + h\nu \rightarrow OH + NO_2$	
$H_2O_2 + h\nu \rightarrow 2\ OH$	
$HCl + h\nu \rightarrow Cl + H$	
$ClONO_2 + h\nu \rightarrow ClO + NO_2$	
$CF_2Cl_2 + h\nu \rightarrow 2\ Cl$	
$CFCl_3 + h\nu \rightarrow 3\ Cl$	
$N_2O_5 + h\nu \rightarrow 2\ NO_2 + O$	GRAHAM and JOHNSTON (1978)
$NO_3 + h\nu \rightarrow NO_2 + O$	GRAHAM and JOHNSTON (1978)
$NO_3 + h\nu \rightarrow NO + O_2$	GRAHAM and JOHNSTON (1978)

Table 4. Twenty-four hour average column rates (15 to 45 km) in units of 10^{11} molecules cm^{-2} s^{-1}. Spring NH, fall SH (south pole is -90°).

Lat.	Prod. O_3 $2\ j[O_2]$	Loss of O_3		Ratio L/P		
		O_x $2\ k[O][O_3]$	NO_x $2\ k[O][NO_2]$	O_x	NO_x	Both
-80	14	2	28	0.13	1.95	2.08
-70	33	3	20	0.09	0.61	0.70
-60	51	5	21	0.11	0.40	0.51
-50	67	9	26	0.14	0.39	0.53
-40	81	13	49	0.16	0.60	0.76
-30	94	14	64	0.15	0.68	0.83
-20	106	16	47	0.15	0.44	0.59
-10	112	17	36	0.15	0.32	0.47
0	119	16	35	0.13	0.29	0.42
10	117	16	37	0.13	0.31	0.44
20	110	14	45	0.13	0.41	0.54
30	100	13	53	0.13	0.53	0.66
40	83	12	44	0.15	0.53	0.68
50	67	9	39	0.13	0.58	0.71
60	48	5	32	0.11	0.66	0.77
70	28	3	26	0.11	0.93	1.04
80	9	2	20	0.19	2.18	2.37

Table 5. Global-sum column rates over various altitude bands, in units of 10^{29} molecules s^{-1}. Spring NH, fall SH.

Alt. Band km	Prod. O_3 $2\ j[O_2]$	Loss of O_3		Ratio L/P		
		O_x	NO_x	O_x	NO_x	Both
45-50	140.2	32.4	9.2	0.23	0.07	0.30
40-45	171.2	42.4	45.2	0.25	0.26	0.51
35-40	155.4	19.0	89.2	0.12	0.57	0.69
30-35	104.0	7.2	57.4	0.07	0.55	0.62
25-30	43.4	2.6	15.4	0.06	0.35	0.41
20-25	8.8	0.52	1.8	0.06	0.30	0.36
15-20	0.9	0.04	0.12	0.04	0.13	0.17
15-45	484	72	209	0.15	0.43	0.58

Table 6. Comparison of four seasons in terms of global instantaneous rates between 15 and 45 km. The total daytime NO_2 is summed over the sunlit hemisphere.

Season NH	$P(O_3)$ s^{-1} (10^{29})	Total Daytime NO_2 (10^{32})	$L(NO_x)$ (10^{29})	$\frac{L}{P}$
SP	484	146	209	0.43
SU	449	119	222	0.50
F	480	135	187	0.39
W	527	134	228	0.43

Table 7. Sensitivity test where NO_2 columns of Figures 1 and 2 are scaled by 2/3 and 4/3. Global instantaneous rates between 15 and 45 km.

A. Summer in NH. Production of O_3 = 449 x 10^{29} s^{-1}. Loss of O_3 from O_x = 75 x 10^{29} s^{-1}.

Rel. NO_2	Total Daytime NO_2 molecules	Loss of O_3 from NO_x s^{-1}	$\frac{L}{P}$
2/3	8.15(33)	145(29)	0.32
1	1.19(34)	222(29)	0.50
4/3	1.55(34)	297(29)	0.66

B. Fall in NH. Production of O_3 = 480 x 10^{29} s^{-1}. Loss of O_3 from O_x = 77 x 10^{29} s^{-1}.

2/3	1.00(34)	127(29)	0.26
1	1.35(34)	187(29)	0.39
4/3	1.95(34)	295(29)	0.61

List of Figures

Figure 1. Temperature in the troposphere and stratosphere. The south pole is -90° and the north pole is 90°. One panel is the average of DÜTSCH'S (1978) values for March, April, May; the other is the average of Dec., Jan., Feb.

Figure 2. Ozone mixing ratios (parts per million by volume).

Figure 3. Ozone concentration in units of 10^{12} molecules cm^{-3}.

Figure 4. Atomic oxygen concentration, 12 hour, daytime average. 3E9 = 3 x 10^{9}.

Figure 5. Observed PM vertical columns of stratospheric nitrogen dioxide, fall-spring: ⊙ NOXON (1979), Figure 1; ⊡ NOXON, Figure 2; △ NOXON, Figure 3; D, HARRIES et al. (1976); C, MURCRAY et al. (1974); B, OGAWA (1979); A, ACKERMAN et al. (1974). The line is that used as the primary case for this study. Sensitivity studies were made with NO_2 columns 2/3 and 4/3 of this line.

Figure 6. Observed PM vertical columns of stratospheric nitrogen dioxide, winter-summer: ⊙, NOXON (1979, Figure 1; △, NOXON, Figure 3; ◇, NOXON, Figure 6. G, GOLDMAN et al. (1978); E, EVANS et al. (1977); F, EVANS et al. (1978); H, DRUMMOND and JARNOT (1979). The line as described in Figure 5.

Figure 7. Nitrogen dioxide profile between 20 and 50 km as observed by DRUMMOND and JARNOT (1978), line A; the integrated vertical column is 2.8×10^{15} molecules cm^{-2}; 44°N, June 1975, one hour after sunrise. Lines B and C represent model NO_2 profiles respectively from 2.4 and 1.0×10^{15} molecules cm^{-2} between 20 and 50 km, one hour after sunrise. The slant lines are mixing ratio by volume.

Figure 8. Ozone photochemical replacement time, the local ozone concentration (Figure 3) divided by the local rate of photochemical formation of ozone (Figure 11).

Figure 9. Daytime average nitrogen dioxide concentrations in units of 10^9 molecules cm^{-3}.

Figure 10. Daytime average nitrogen dioxide mixing ratios in parts per billion by volume.

Figure 11. Rate of ozone production from O_2 photolysis, $P(O_3)$, $2\ j[O_2]$, 24 hour average, in units of molecules cm^{-3} s^{-1}.

Figure 12. Rate of ozone destruction by Chapman reactions, $L(O_x)$, $2\ k[O][O_3]$, 24 hour average, in units of molecules cm^{-3} s^{-1}.

Figure 13. The ratio of the rate of ozone destruction by O_x to the rate of ozone formation by O_2 photolysis. $L(O_x)/P(O_3) = 2\ k[O][O_3]/2\ j[O_2]$.

Figure 14. The rate of ozone destruction by NO_x, $L(NO_x) = 2\ k[O][NO_2]$, in units of molecules cm^{-3} s^{-1}.

Figure 15. Ratio of ozone destruction by NO_x, $L(NO_x)$, to ozone production by photolysis of oxygen, $P(O_3)$.

Figure 16. The ratio $L(NO_x)/P(O_3)$, Figure 14, superimposed on ozone mixing ratios, Figure 2. A, maximum O_3 mixing ratio. B, region of heavy, fast ozone destruction by NO_x. C, maximum rate of O_3 production from oxygen photolysis.

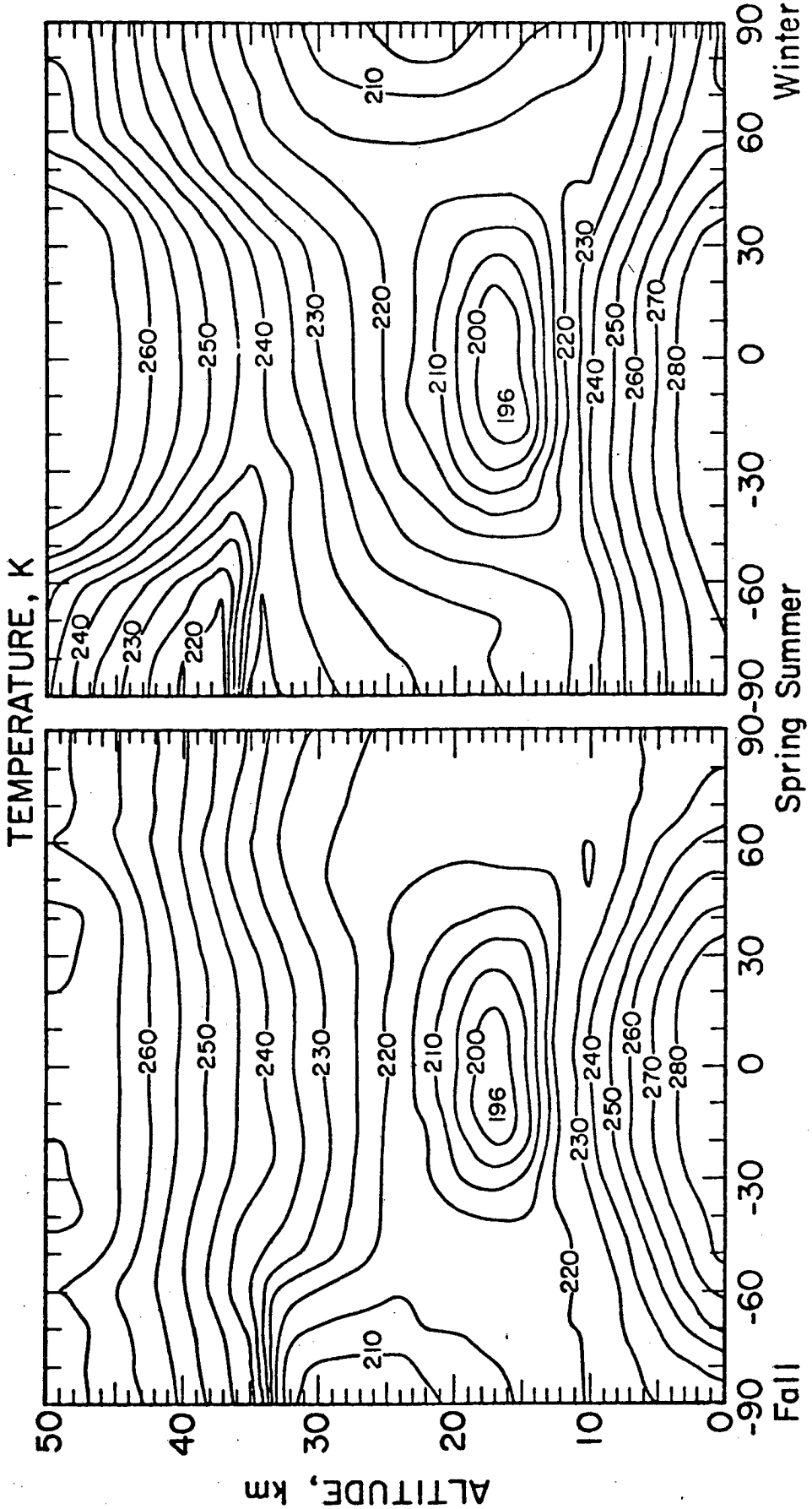
TEMPERATURE, K
ALTITUDE, km
LATITUDE
Fall
Winter
Spring
Summer
-90
-60
-30
0
30
60
90
0
10
20
30
40
50
196
200
210
220
230
240
250
260
270
280

Fig. 1

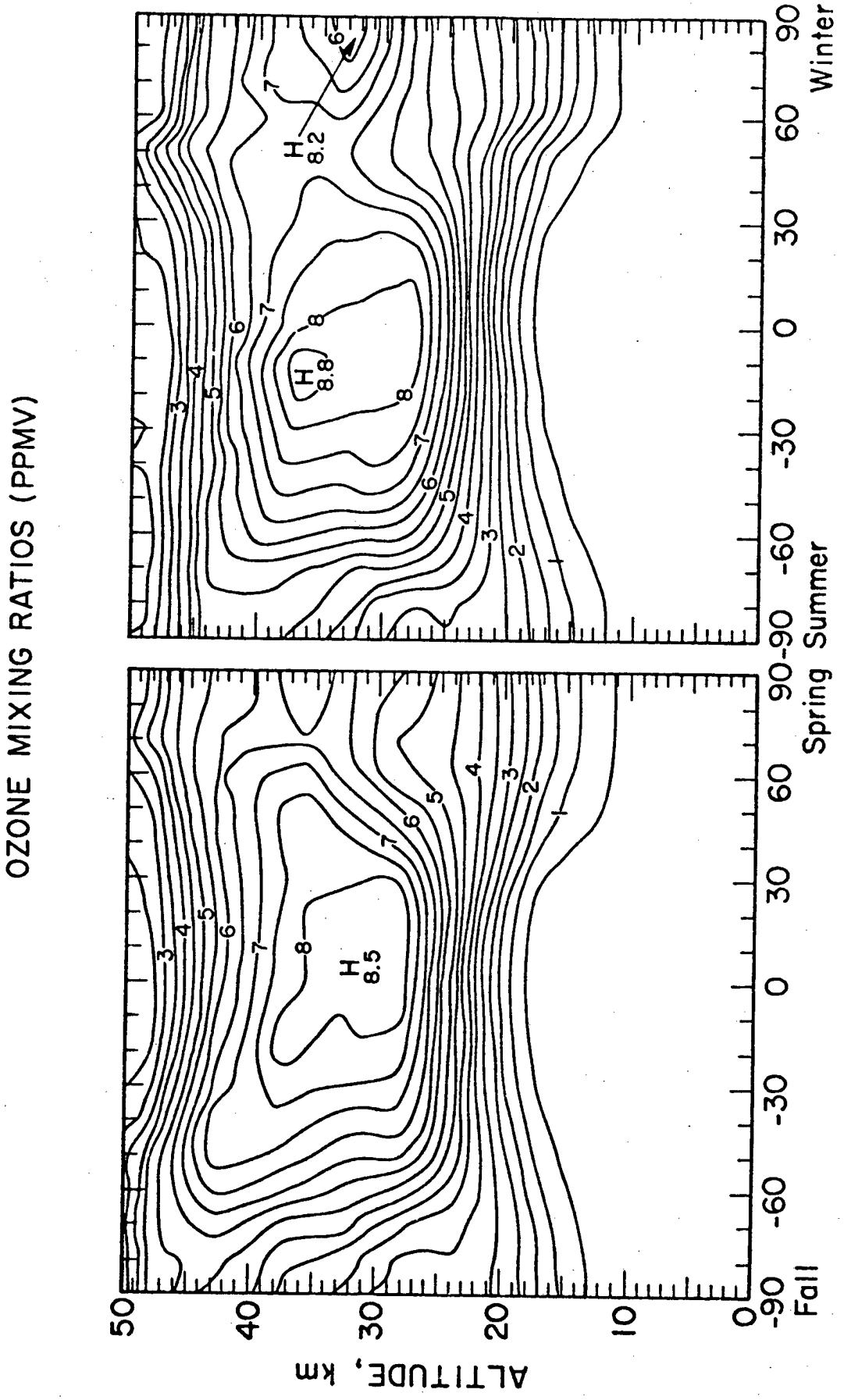
OZONE MIXING RATIOS (PPMV)
ALTITUDE, km
50
40
30
20
10
0
-90
-60
-30
0
30
60
90
LATITUDE
Fall
Spring
Summer
Winter
H
8.5
H
8.8
H
8.2

Fig. 2

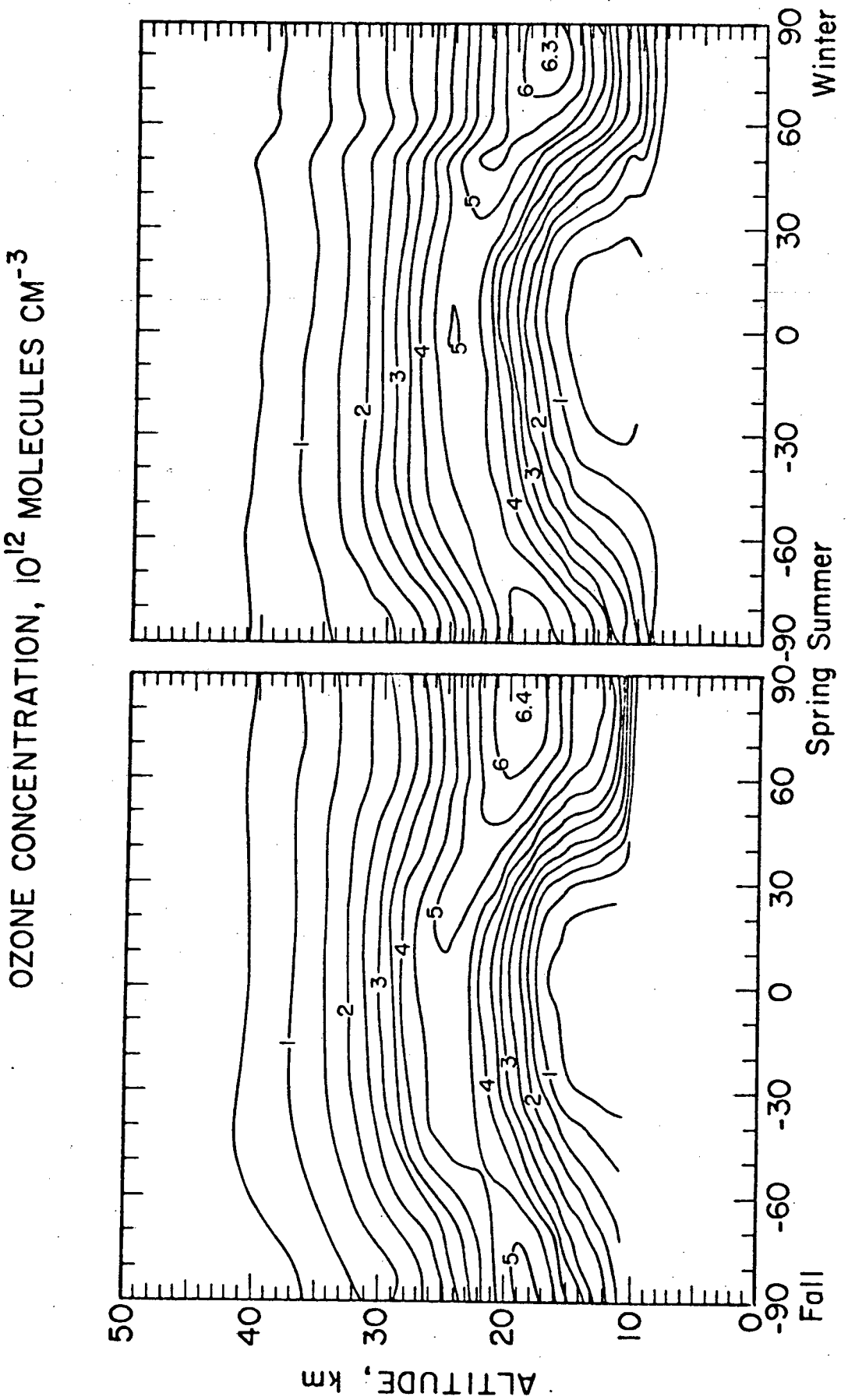
OZONE CONCENTRATION, 10^{12} MOLECULES CM^{-3}
ALTITUDE, km
50
40
30
20
10
0
Fall
Spring
Summer
Winter
LATITUDE
-90
-60
-30
0
30
60
90
1
2
3
4
5
6
6.3
6.4

Fig. 3

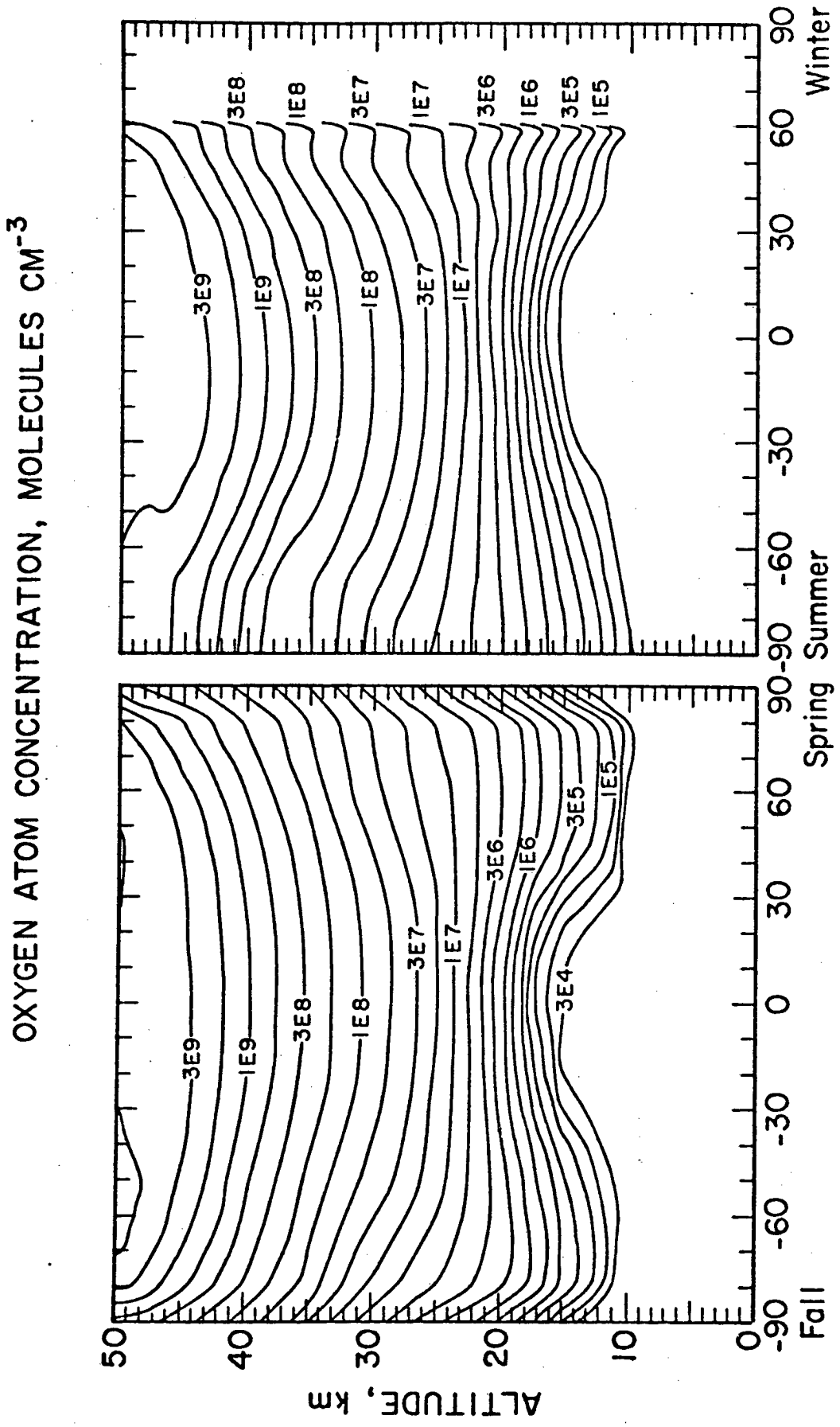
OXYGEN ATOM CONCENTRATION, MOLECULES CM-3
ALTITUDE, km
LATITUDE
Fall
Winter
Spring
Summer
3E9
1E9
3E8
1E8
3E7
1E7
3E6
1E6
3E5
1E5
3E4

Fig. 4

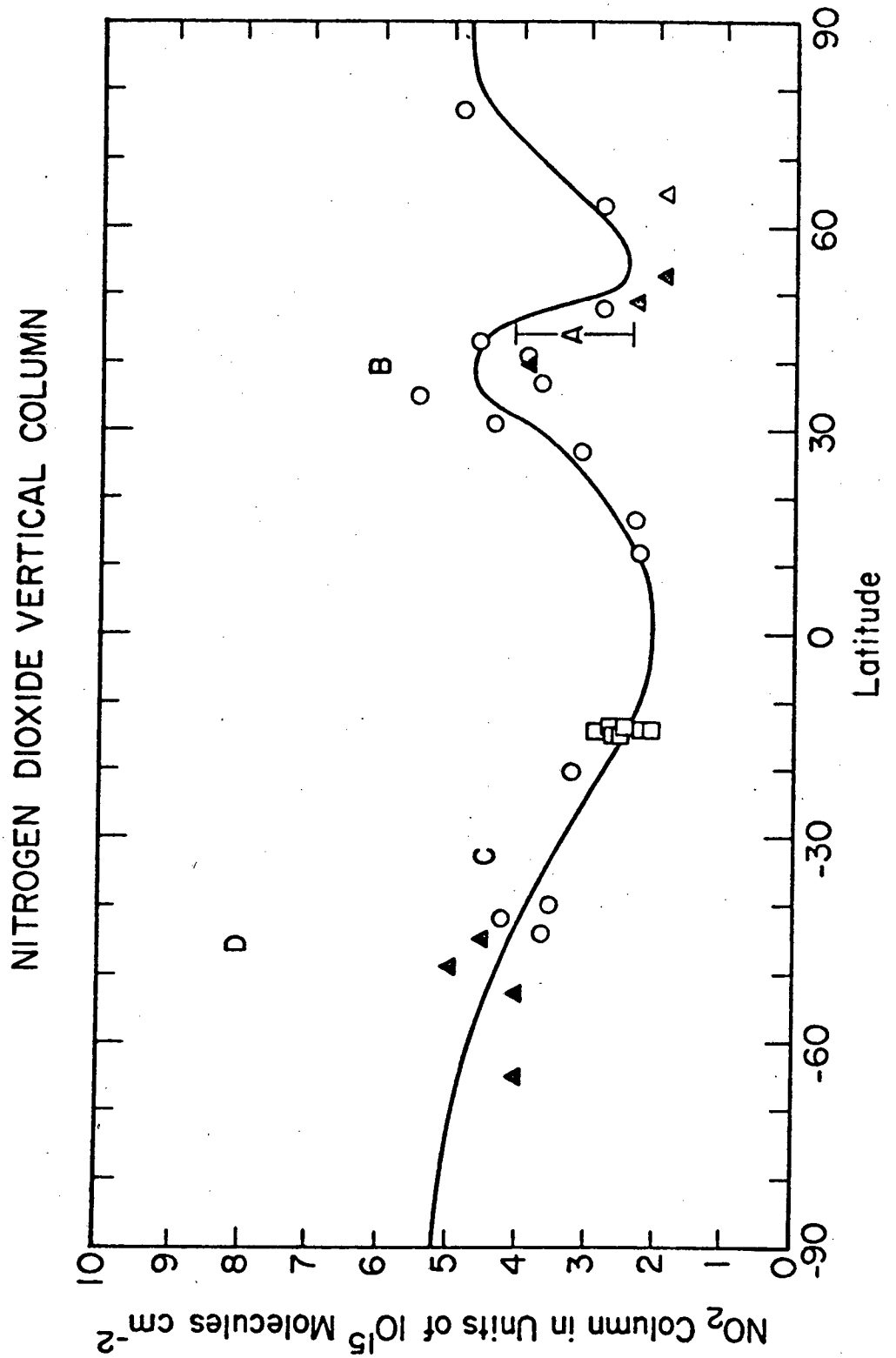
NITROGEN DIOXIDE VERTICAL COLUMN
NO_2 Column in Units of 10^{15} Molecules cm^{-2}
Latitude
-90
-60
-30
0
30
60
90
0
1
2
3
4
5
6
7
8
9
10
A
B
C
D

Fig. 5

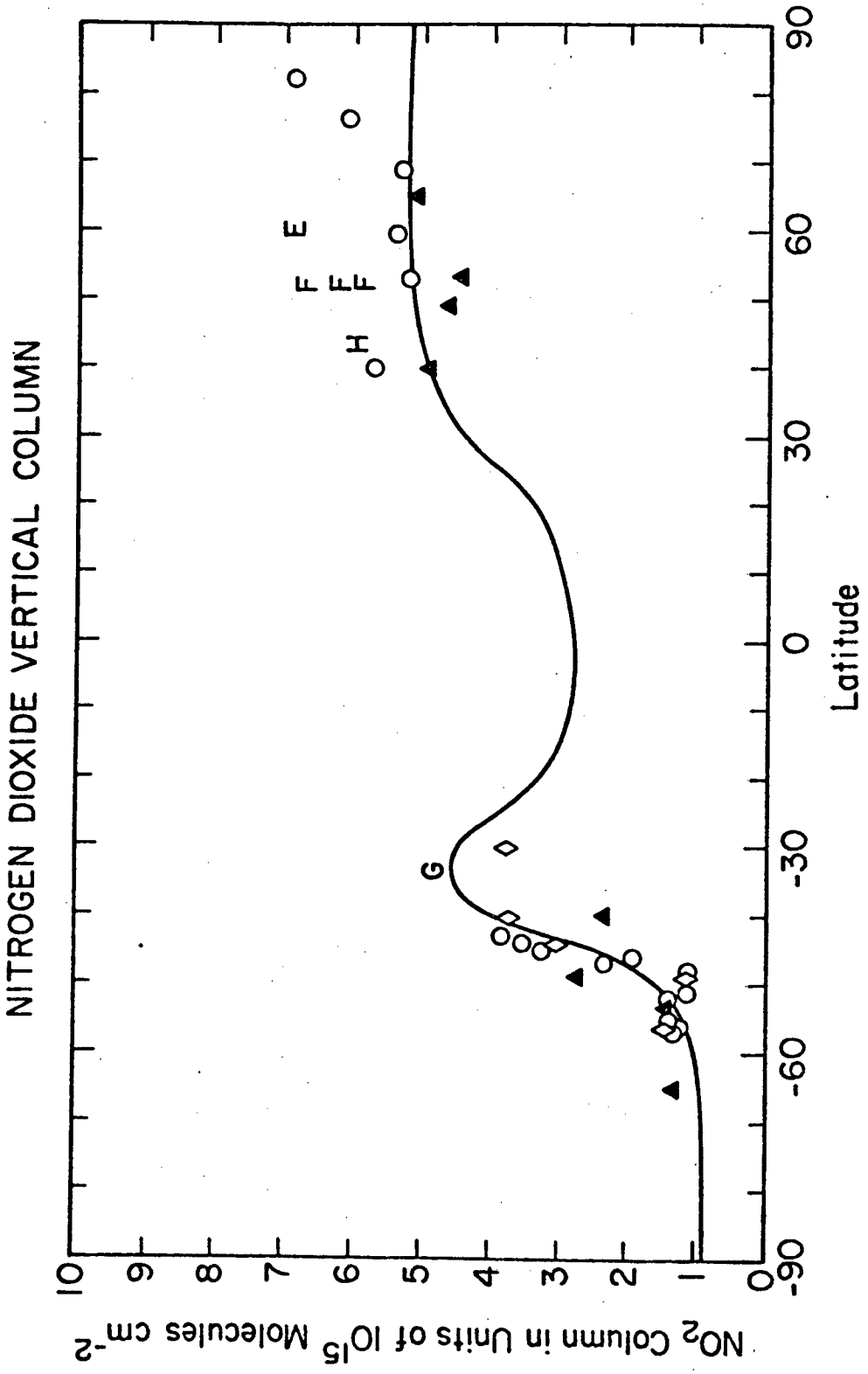
NITROGEN DIOXIDE VERTICAL COLUMN
NO2 Column in Units of 10^15 Molecules cm^-2
Latitude
90
60
30
0
-30
-60
-90
0
1
2
3
4
5
6
7
8
9
10
E
F
F
F
H
G

Fig. 6

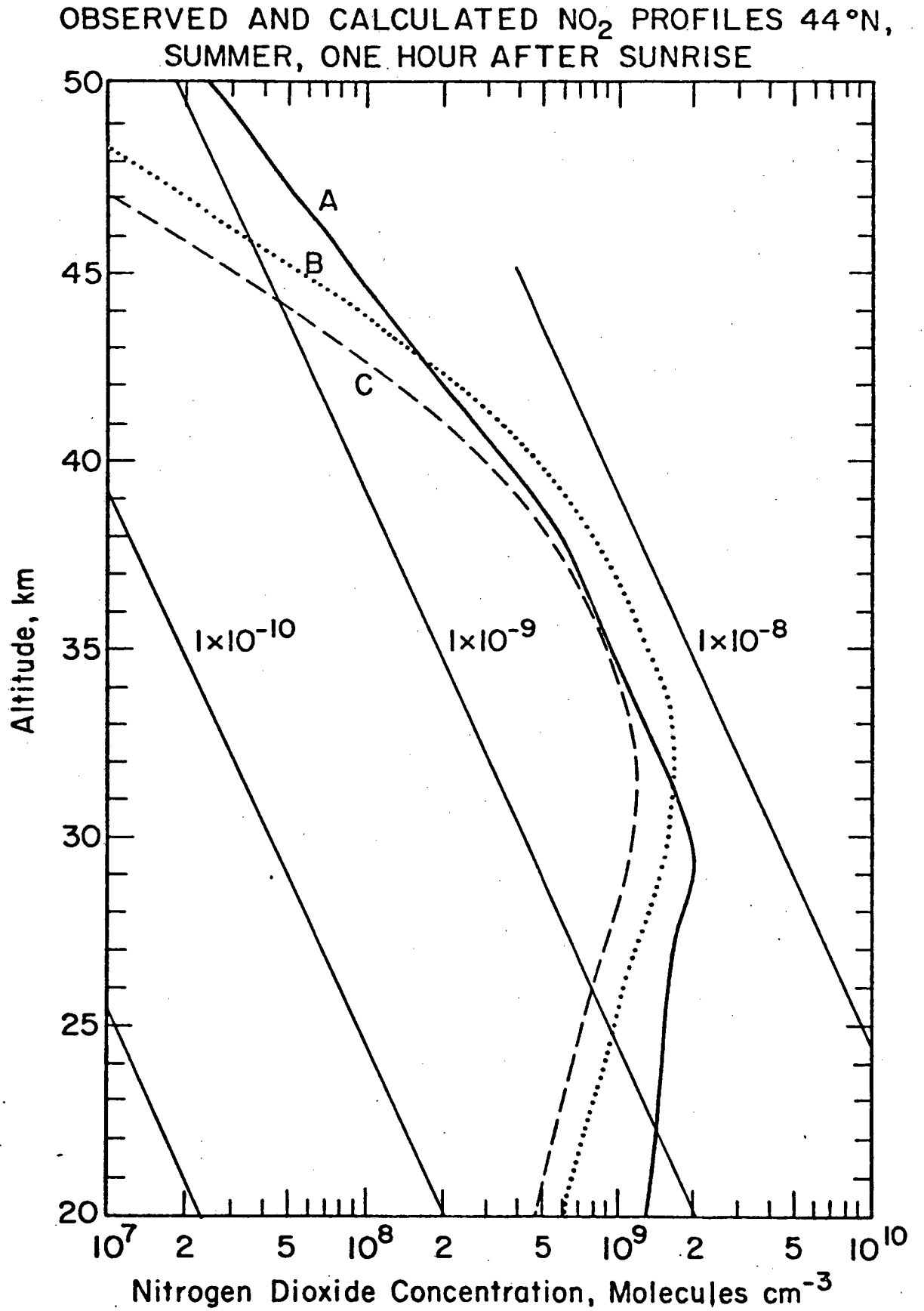
OBSERVED AND CALCULATED NO_2 PROFILES 44°N, SUMMER, ONE HOUR AFTER SUNRISE
Altitude, km
50
45
40
35
30
25
20
A
B
C
1×10⁻¹⁰
1×10⁻⁹
1×10⁻⁸
10⁷ 2 5 10⁸ 2 5 10⁹ 2 5 10¹⁰
Nitrogen Dioxide Concentration, Molecules cm⁻³

Fig. 7

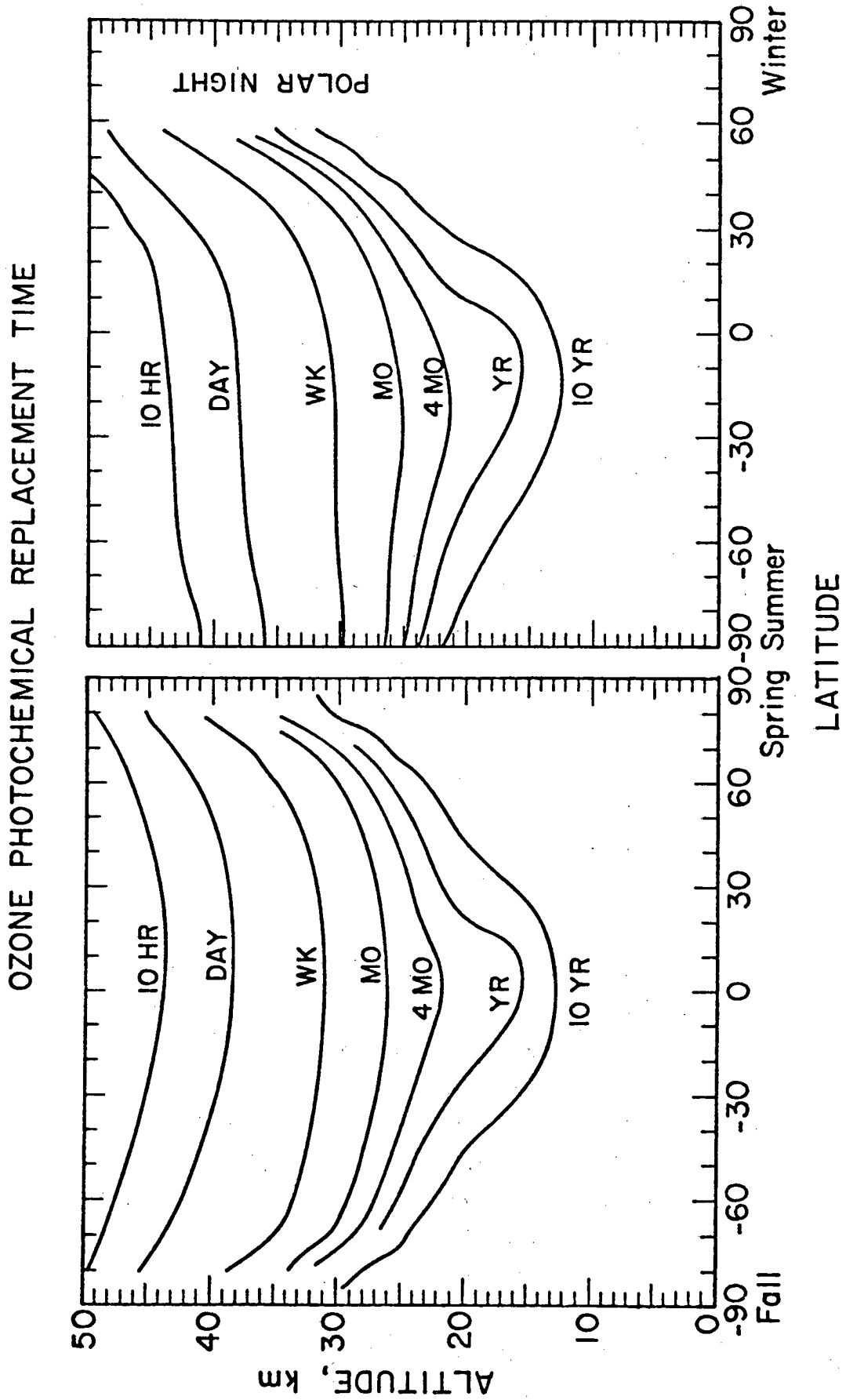
OZONE PHOTOCHEMICAL REPLACEMENT TIME
POLAR NIGHT
10 HR
DAY
WK
MO
4 MO
YR
10 YR
Winter
Spring
Summer
Fall
LATITUDE
ALTITUDE, km
50
40
30
20
10
0
90
60
30
0
-30
-60
-90

Fig. 8

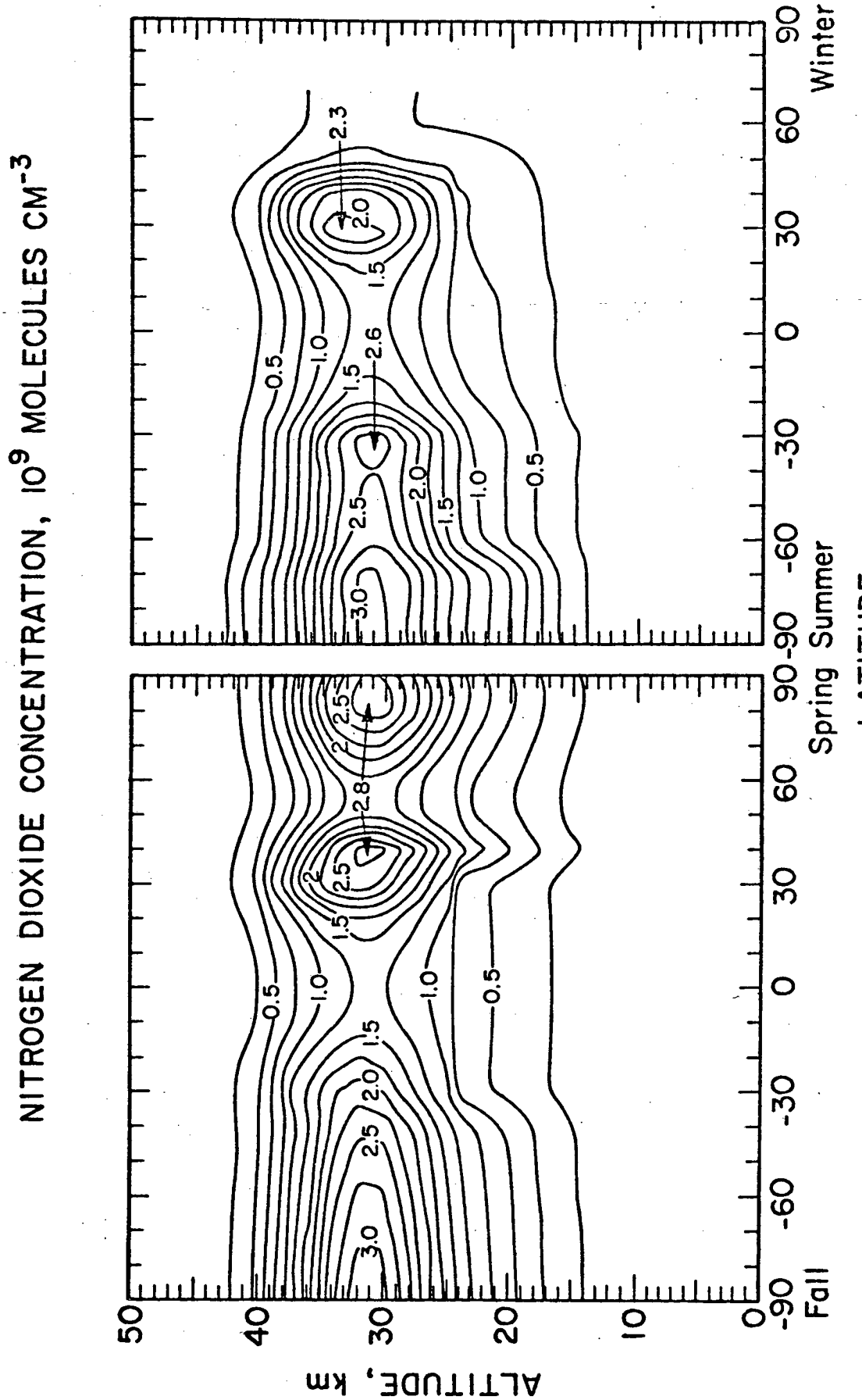
NITROGEN DIOXIDE CONCENTRATION, 10^9 MOLECULES CM^{-3}
ALTITUDE, km
LATITUDE
Winter
Spring Summer
Fall

Fig. 9

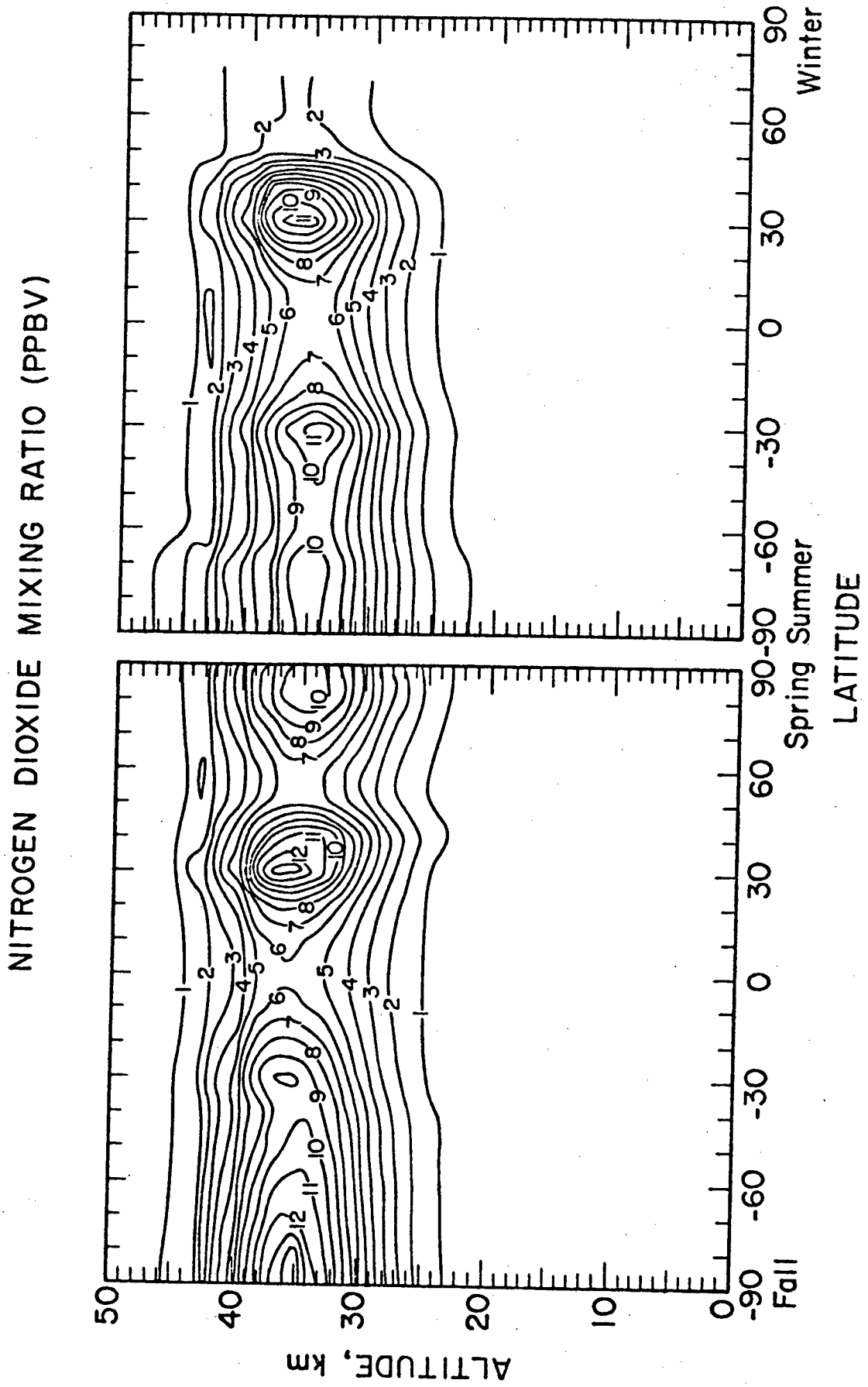
NITROGEN DIOXIDE MIXING RATIO (PPBV)
ALTITUDE, km
LATITUDE
Winter
Spring Summer
Fall
50
40
30
20
10
0
90
60
30
0
-30
-60
-90

Fig. 10

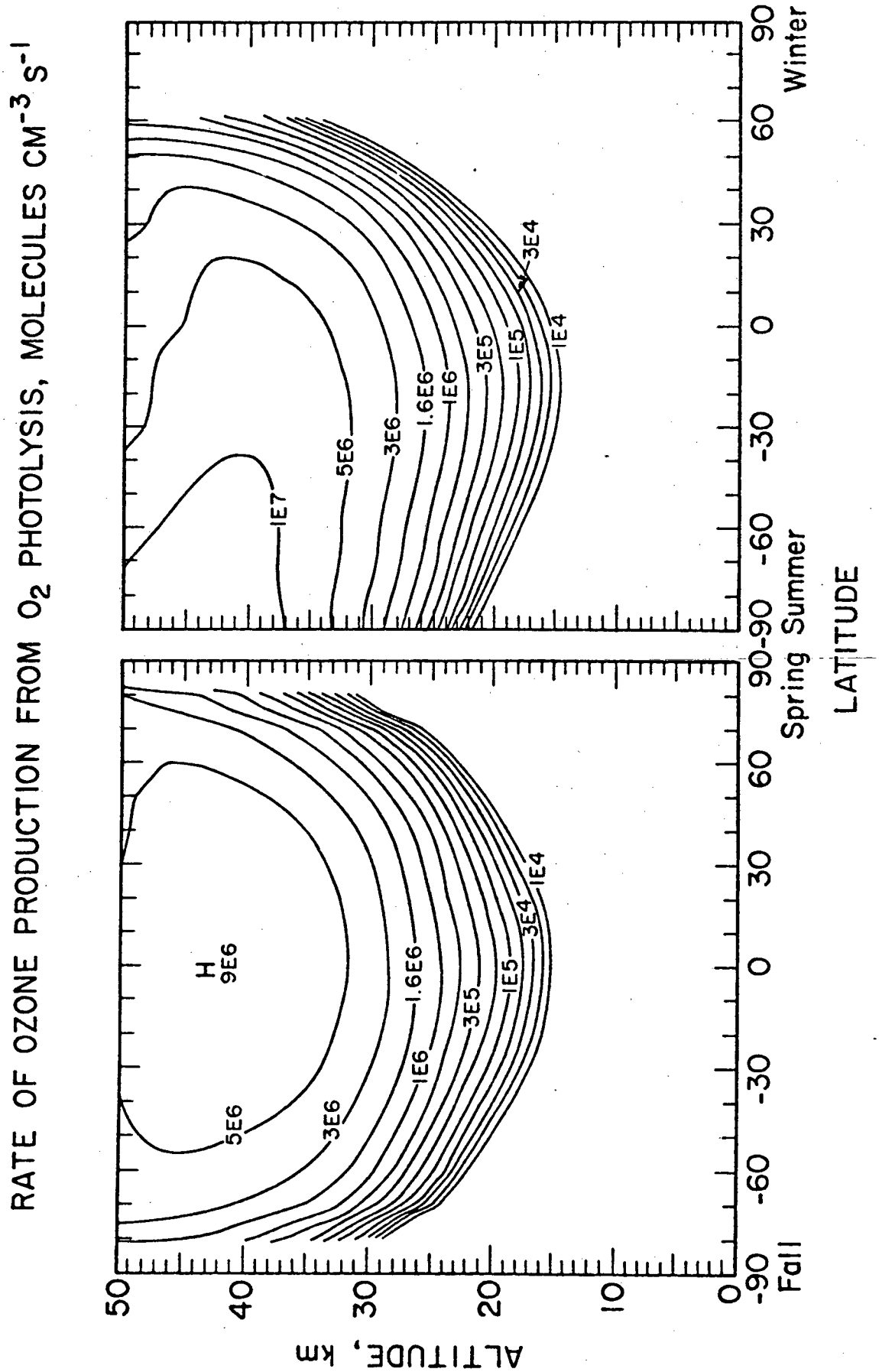
RATE OF OZONE PRODUCTION FROM O_2 PHOTOLYSIS, MOLECULES CM^{-3} S^{-1}
ALTITUDE, km
LATITUDE
Fall
Spring Summer
Winter
H
9E6
5E6
3E6
1.6E6
1E6
3E5
1E5
3E4
1E4
1E7

Fig. 11

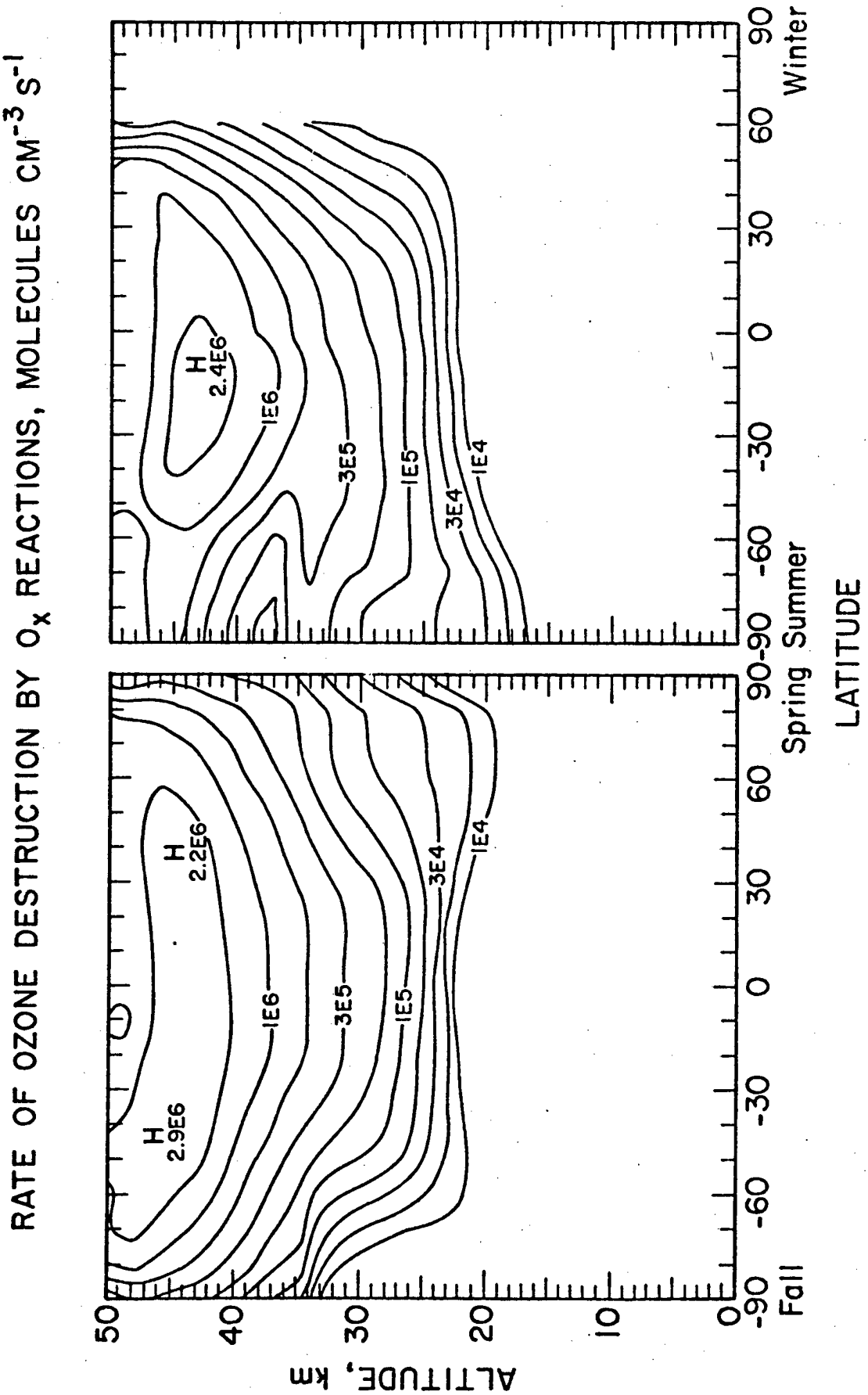
RATE OF OZONE DESTRUCTION BY O_x REACTIONS, MOLECULES CM^{-3} S^{-1}
ALTITUDE, km
LATITUDE
Fall
Winter
Spring
Summer
H
2.9E6
H
2.2E6
H
2.4E6
1E6
3E5
1E5
3E4
1E4
50
40
30
20
10
0
-90
-60
-30
0
30
60
90

Fig. 12

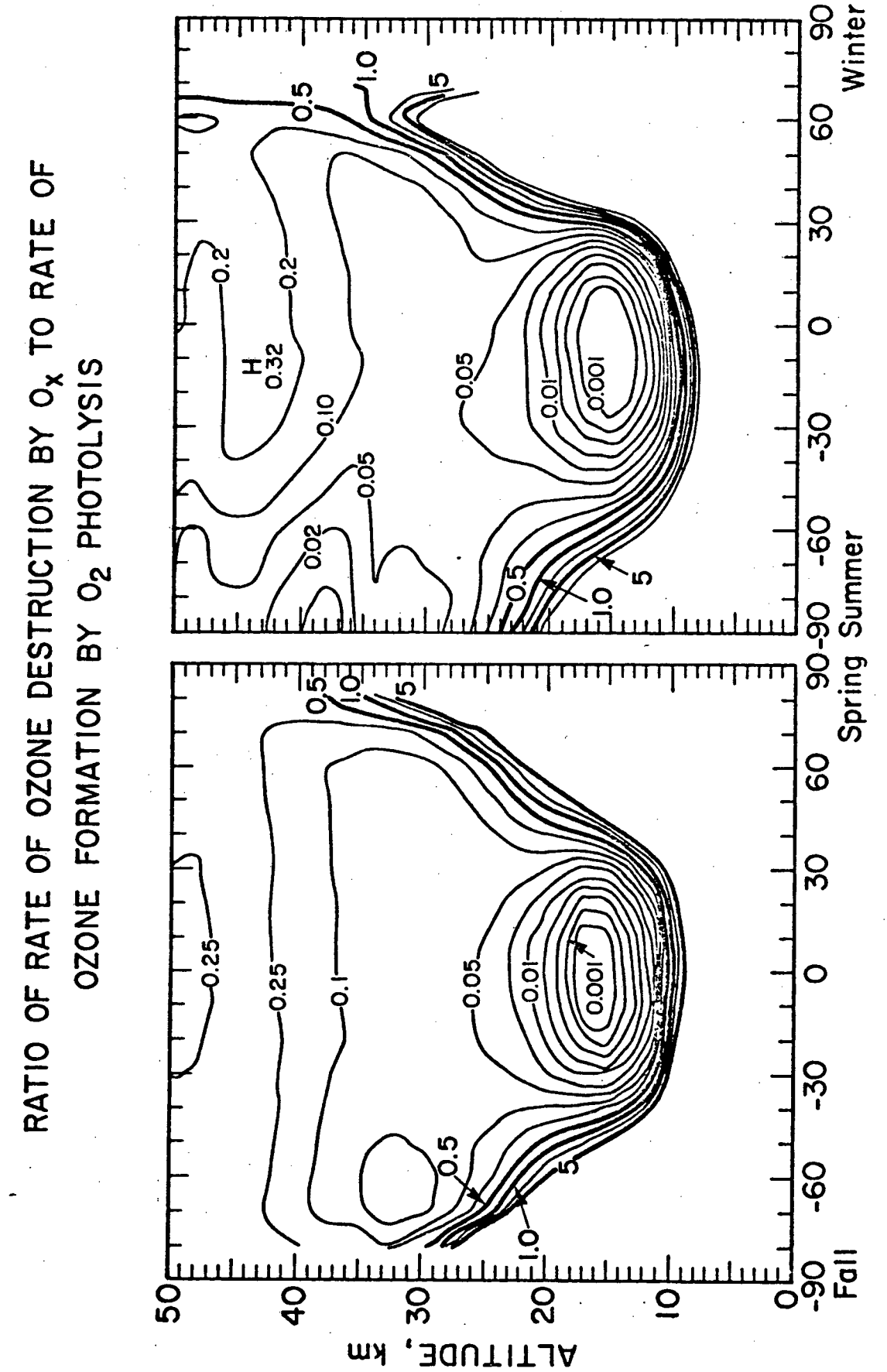
RATIO OF RATE OF OZONE DESTRUCTION BY O_x TO RATE OF OZONE FORMATION BY O_2 PHOTOLYSIS
ALTITUDE, km
LATITUDE
Winter
Spring Summer
Fall
H
0.32
0.2
0.5
1.0
5
0.10
0.05
0.02
0.01
0.001
0.25
0.1

Fig. 13

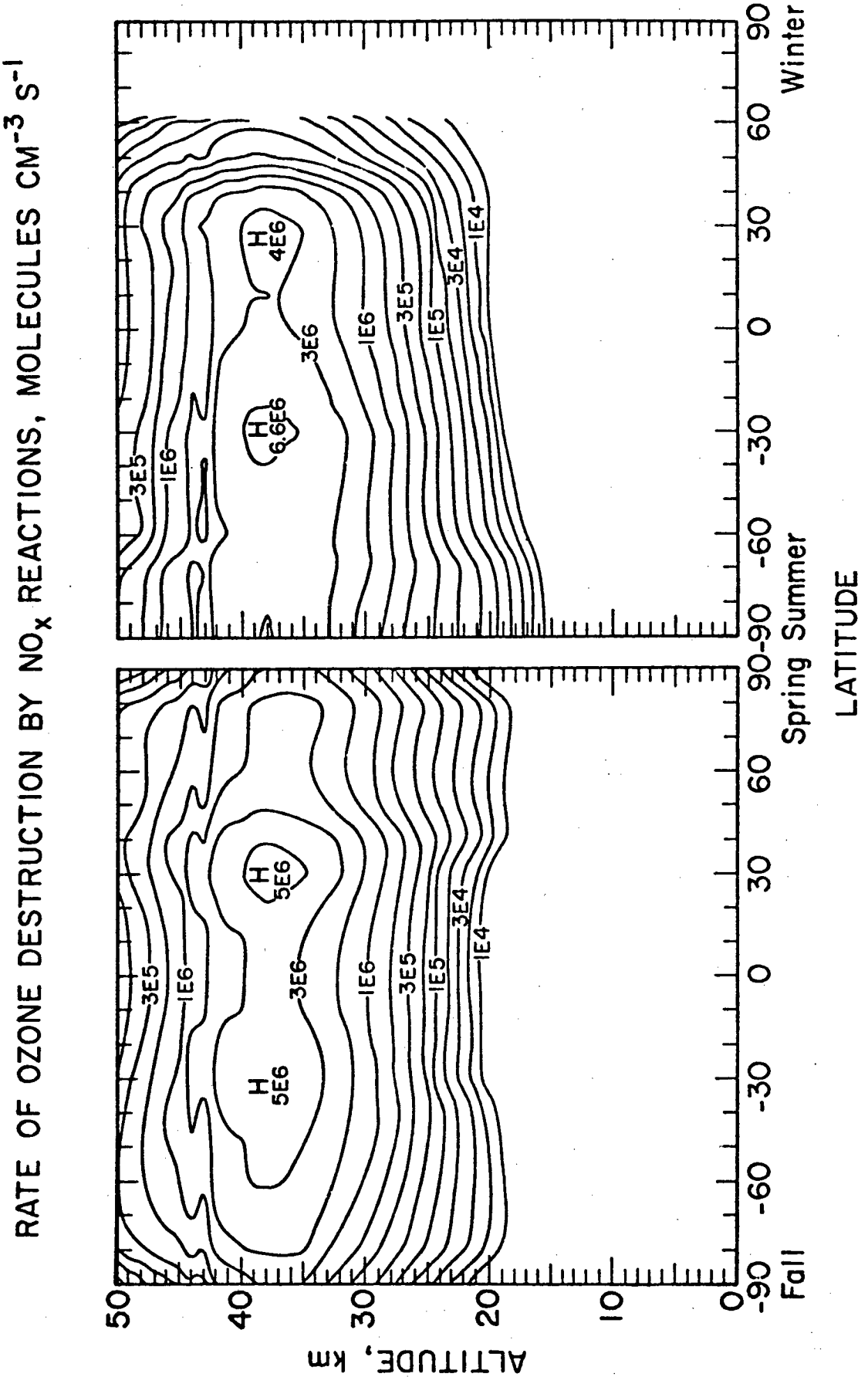
RATE OF OZONE DESTRUCTION BY NO_x REACTIONS, MOLECULES CM^{-3} S^{-1}
ALTITUDE, km
LATITUDE
Fall
Winter
Spring
Summer
H 5E6
H 5E6
H 6.6E6
H 4E6
3E5
1E6
3E6
1E6
3E5
1E5
3E4
1E4
50
40
30
20
10
0
-90
-60
-30
0
30
60
90

Fig. 14

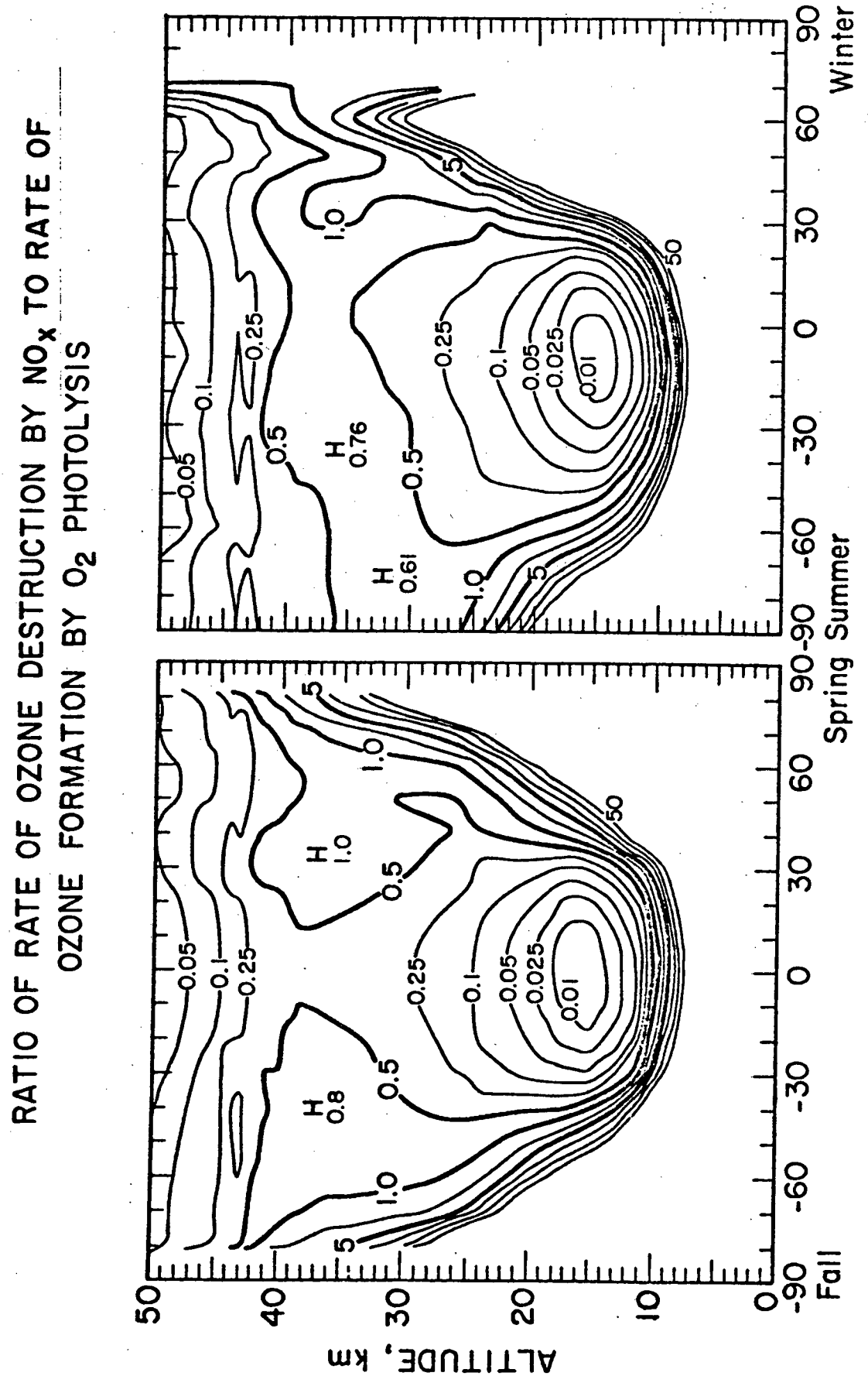
RATIO OF RATE OF OZONE DESTRUCTION BY NO_x TO RATE OF OZONE FORMATION BY O_2 PHOTOLYSIS
ALTITUDE, km
LATITUDE
Fall
Spring Summer
Winter
H 0.8
H 1.0
H 0.61
H 0.76
0.05
0.1
0.25
0.5
1.0
5
50
0.01
0.025
0.05
0.1
0.25
0.5
1.0
5
50
-90
-60
-30
0
30
60
90
0
10
20
30
40
50

Fig. 15

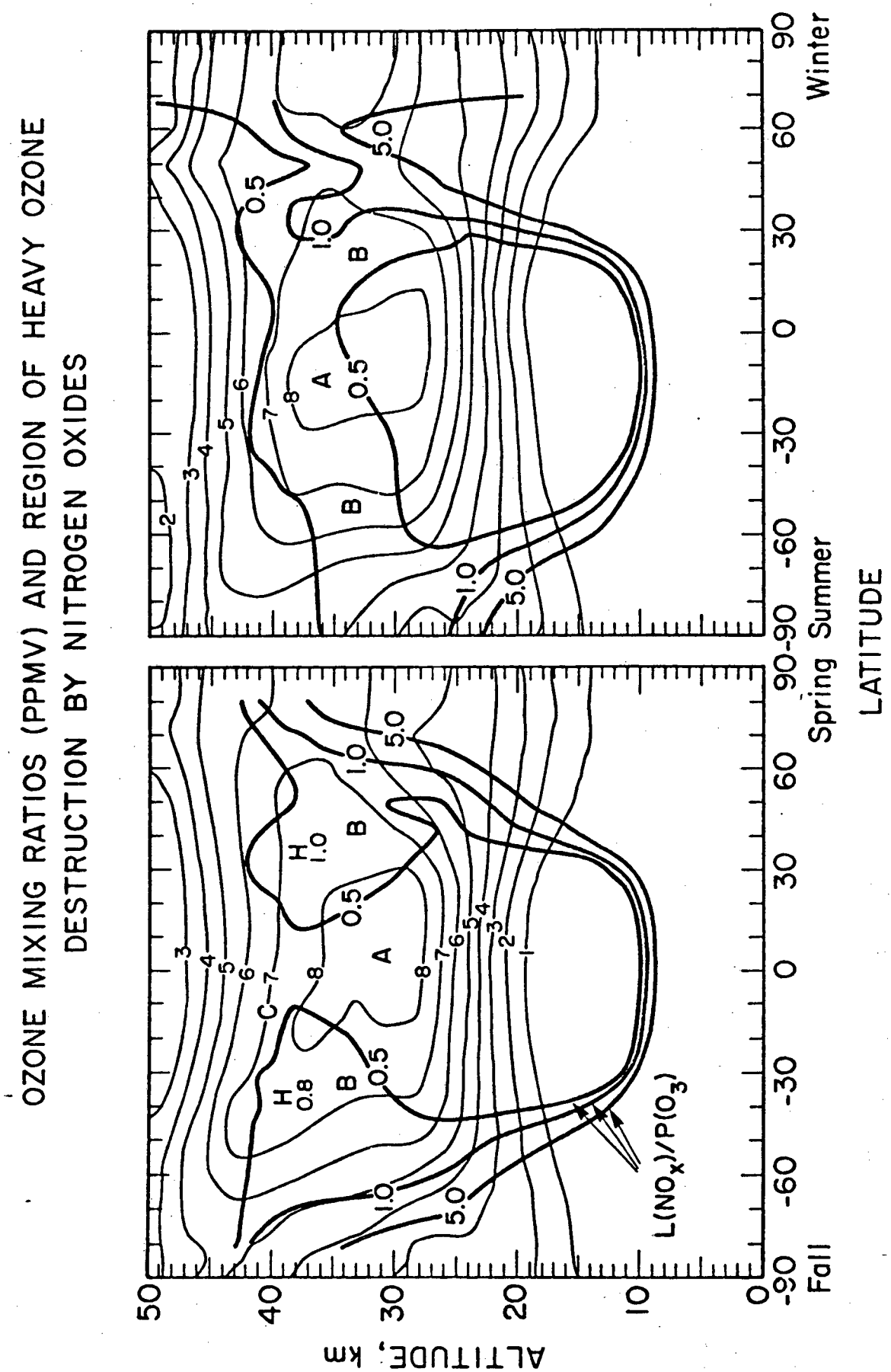
OZONE MIXING RATIOS (PPMV) AND REGION OF HEAVY OZONE
DESTRUCTION BY NITROGEN OXIDES
ALTITUDE, km
LATITUDE
Fall
Winter
Spring
Summer
$L(NO_x)/P(O_3)$
A
B
C
H 0.8
H 1.0
0.5
1.0
5.0

Fig. 16

TECHNICAL INFORMATION DEPARTMENT
LAWRENCE BERKELEY LABORATORY
UNIVERSITY OF CALIFORNIA
BERKELEY, CALIFORNIA 94720